

IMPLEMENTATION OF 5G TECHNOLOGIES WITH  
HETEROGENEOUS COOPERATIVE SPECTRUM SENSING AND LTE-R

by

Kuldeep S. Gill

A Thesis  
Submitted to the Faculty  
of the  
WORCESTER POLYTECHNIC INSTITUTE  
in partial fulfillment of the requirements for the  
Degree of Master of Science  
in  
Electrical and Computer Engineering  
by

---

December 2017

APPROVED:

---

Professor Alexander Wyglinski, Major Advisor

---

Professor Kaveh Pahlavan

---

Dr. Travis Collins

## Abstract

There have been an unprecedented increase in demand for high data rates and mobility required by new wireless applications which has led to intensive research on fifth generation (5G) wireless communication system. By 2020, 5G is projected to be employed worldwide supporting the connectivity of up to 20 billion devices and will be crucial in the success of vehicular networking and internet of things (IoT). It is also believed that 5G systems would be capable of providing significant improvements in cell capacity and will support high data rates up to 5 and 50 Gb/s for high-mobility and pedestrian users, respectively. However, to achieve such data rates for high-mobility scenarios there are still many challenges for wireless system engineers.

In this thesis, we propose two test-beds namely Heterogeneous Cooperative Spectrum Sensing (CSS) and Long Term Evolution for Railways (LTE-R) performance analysis test-bed to further advance the 5G system development. Heterogeneous CSS test-bed is implemented using Software-Defined Radios (SDRs) with different radio characteristics. We used both soft and hard data fusion schemes to compare the signal source detection performance in real-time fading scenario. For 5G technologies, the most effective solution is to use the underutilized spectrum as a secondary user via dynamic spectrum access (DSA). It is very challenging to get an accurate estimate of incumbent users with a single-sensor system under a practical fading environment. Various non-idealities such as shadowing, multipath and fluctuating noise variance can make it difficult to detect the primary user. Cooperative spectrum sensing can mitigate the effects of multipath and shadowing by utilizing the spatial and temporal diversity of a multiple radio network. LTE-R test-bed analyze the performance of high speed trains (HSTs) in a tunnel environment and can be used to test 5G systems for high mobility scenario in drastically impaired channels.

## Acknowledgements

I would like to express my deepest gratitude to my advisor Professor Alexander Wyglinski for his continuous guidance and support towards my course of degree. I am very thankful for the opportunity to work with him in Wireless Innovation Laboratory at Worcester Polytechnic Institute.

I want to thank Professor Kaveh Pahlavan and Dr. Travis Collins for serving on my committee and providing valuable suggestions and comments with regards to my thesis.

I would also like to thank my WILab team members Dr. Srikanth Pagadarai, Dr. Paulo Ferreira, Renato, Le and my friends Rasika, Devdip and Raunak for their immense support during my graduate studies. Finally, I'm also thankful to my parents, without their constant support I wouldn't be here.

# Contents

<b>List of Figures</b>	<b>5</b>
<b>List of Tables</b>	<b>7</b>
<b>1 Introduction</b>	<b>8</b>
1.1 Motivation . . . . .	8
1.2 State of the Art . . . . .	10
1.3 Thesis Contributions . . . . .	12
1.4 Thesis Organization . . . . .	12
<b>2 Introduction to 5G and Key Technologies</b>	<b>14</b>
2.1 5G Cellular Architecture . . . . .	15
2.2 Key Technologies of 5G System . . . . .	18
2.2.1 Massive MIMO . . . . .	19
2.2.2 Machine-to-Machine (M2M) Communication . . . . .	21
2.2.3 Spectrum Regulation for 5G . . . . .	24
2.3 5G using Millimeter Wave (mmWave) . . . . .	26
2.4 Vehicular Communication Using 5G . . . . .	28
2.5 Summary . . . . .	30
<b>3 Heterogeneous Cooperative Spectrum Sensing (CSS)</b>	<b>31</b>
3.1 Cognitive Radios . . . . .	31
3.2 CSS in Heterogeneous Networks . . . . .	33
3.3 Software Defined Radios . . . . .	35
3.3.1 USRP N210 and RTL-SDR . . . . .	36
3.3.2 GNU Radio and Software-Defined Radio . . . . .	37
3.3.3 MATLAB . . . . .	38
3.4 Summary . . . . .	38
<b>4 Long Term Evolution for Railways (LTE-R)</b>	<b>40</b>
4.1 LTE-R Communication System . . . . .	40
4.2 Leaky Coaxial Cable for LTE-R . . . . .	43
4.3 Channel Impairments Inside a Tunnel . . . . .	45
4.3.1 Multipath Fading . . . . .	45

4.3.2	Doppler Shift . . . . .	46
4.4	Proposed Channel Model . . . . .	47
4.5	Summary . . . . .	49
<b>5</b>	<b>Implementation</b>	<b>50</b>
5.1	Overview . . . . .	50
5.2	Experimental Setup for Heterogeneous CSS . . . . .	51
5.2.1	Sensor Node and Signal Source Setup . . . . .	53
5.3	Hard-Data Fusion Scheme . . . . .	55
5.4	Soft-Data Fusion Scheme . . . . .	55
5.4.1	Maximum Normalized Energy Scheme . . . . .	56
5.4.2	Equal Gain Combining Scheme . . . . .	57
5.5	LTE-R Testbed in Matlab . . . . .	58
5.6	Summary . . . . .	60
<b>6</b>	<b>Experimental Results</b>	<b>61</b>
6.1	Overview . . . . .	61
6.2	Heterogeneous CSS Results . . . . .	61
6.2.1	Hard Decision Combining . . . . .	62
6.2.2	Soft Decision Combining . . . . .	62
6.3	HST LTE-R in a Tunnel . . . . .	63
6.3.1	K-factor in a Tunnel . . . . .	64
6.3.2	BER Performance . . . . .	64
6.4	Summary . . . . .	67
<b>7</b>	<b>Conclusions</b>	<b>69</b>
7.1	Research Outcomes . . . . .	69
7.2	Future Work . . . . .	70
<b>Bibliography</b>		<b>71</b>
<b>A</b>	<b>Appendix: Heterogeneous Cooperative Spectrum Sensing Code</b>	<b>79</b>
A.1	harddecisionpdroc.m . . . . .	79
A.2	softharddecisionpd.m . . . . .	81
A.3	spectrumsenseusrp.py . . . . .	83
A.4	gnuradiortlsdrsense.py . . . . .	91
<b>B</b>	<b>Appendix: LTE-R Analysis Code</b>	<b>97</b>
B.1	kfactordist.m . . . . .	97
B.2	bercalculation.m . . . . .	98

# List of Figures

1.1	Heterogeneous sensor network employing cooperative spectrum sensing. $RFFE_i$ and $SR_i$ represents different front end and sampling rates for the SDR units.	9
1.2	High speed train inside a tunnel for LTE-R. $D_{LOS}$ is the distance between transmitter and receiver, $d$ is the distance between the LCX cable transmission slots.	11
2.1	5G Architecture . . . . .	16
2.2	Massive-MIMO implementation using patch antenna arrays . . . . .	20
2.3	Beamforming for $N=4, 8, 12$ and $16$ linear dipole antenna elements. As the number of antenna element increases we see a sharper beam confined in a smaller region. Massive-MIMO can utilize beamforming to increase spatial gain and spectral efficiency. . . . .	21
2.4	Machine-to-Machine communication paradigm in 5G Cellular System. . . . .	22
2.5	Machine-to-Machine communication paradigm in 5G Cellular System. . . . .	25
2.6	Large-scale propagation loss for $f_c = 1$ GHz, $10$ GHz, $28$ Ghz and $60$ GHz. . . . .	27
2.7	Vehicular communication using D2D 5G cellular communication technology. . . . .	29
3.1	The block diagram explaining the basic parts of Cognitive Radio system. The operating parameters are configured based on the characterization of the wireless environment. . . . .	32
3.2	Software defined radio pushes all the adaptive elements and data manipulation operation into software. The goal of SDR is to provide or define all of the radio operation in software. . . . .	35
3.3	GNURadio and Software-Defined Radio . . . . .	38
4.1	Proposed LTE-R Architecture for next generation High-speed Railways consisting of EPA and E-UTRAN. . . . .	41
4.2	Leaky Coaxial Cable . . . . .	44
4.3	Doppler spectrum for LTE-R at different train velocities $v$ (km/h) = 300, 400 and 500 and $f_c = 5$ GHz. . . . .	47
4.4	HST channel model consisting of time-series K-factor and Doppler shift caused due to velocity of the train. . . . .	48

5.1	Experimental Test-Bed For Cooperative Sensing in Heterogeneous Network. Sensors 1, 2 and 4 are RTL-SDR units, sensor 3 is USRP N210 and TX is another USRP N210 unit which is used as a signal source for this work. . . . .	52
5.2	GNU Radio Flowgraph For Transmitter Running on USRP N210. . . . .	54
5.3	GNURadio Flowgraph For USRP and RTL-SDR sensor nodes. . . . .	54
5.4	Flowchart showing AND, OR and Majority Rule Fusion schemes. . . . .	56
5.5	Flowchart describing Maximum Normalized Energy Scheme in detail. . . . .	57
5.6	Flowchart describing Equal Gain Combining Scheme in detail. . . . .	58
5.7	Block diagram of a communication system through a HST channel using QPSK, 16-QAM and 64-QAM. . . . .	59
6.1	Probability of Detection versus $SNR_{avg}$ For Hard Decision Combining. . .	63
6.2	ROC Characteristics for Hard Decision Combining with Different SNRs. . .	64
6.3	Probability of Detection versus $SNR_{avg}$ For Soft and Hard Decision Com- bining. . . . .	65
6.4	Received LTE-R OFDM signal under HST Ricean Fading Environment. . .	66
6.5	K-factor versus $D_{LOS}$ for different center frequencies $f_c = 2, 3$ and 5 GHz. .	66
6.6	Comparison of $E_b/N_0$ verus BER for LTE-R OFDM modulation with dif- ferent $K$ -factors. The first three sub-figures shows the $E_b/N_0$ versus BER for individual modulation schemes employed in LTE-R and in last plot we compare all the modulation schemes for different $K$ -factors. . . . .	67
6.7	BER variation with time for HST with different modulation schemes of LTE- R. As the train moves towards the antenna the general trend of BER goes down with small-scale fluctuations due to varying K-factor. . . . .	68

# List of Tables

2.1	Cellular Technologies Comparison between different generations of deployed digital cellular networks. Data rates, standard and implementation technology is compared for the 3G, 4G and 5G . . . . .	15
4.1	Comparison of system parameters between GSM-R , LTE and LTE-R. . . . .	42
5.1	Operating Characteristics of Sensor Nodes . . . . .	54
5.2	Tunnel and Tx/Rx Characteristics . . . . .	59

# Chapter 1

## Introduction

### 1.1 Motivation

There has been an exponential growth in the Internet landscape. The devices like smartphones, computers, laptops, tablets will continue to increase along with multitude of other devices that are connected to Internet. This has facilitated the research in dynamic spectrum access (DSA) [1, 2] for efficient utilization of spectrum resources to sustain billions of Internet of Things (IoT) devices. There has been a significant increase in the study of cognitive radios for efficiently utilizing the electromagnetic spectrum. It has been observed that the spectrum occupancy is not uniform across all frequency bands, resulting in numerous spectral white spaces [3]. To opportunistically access the idle channel, spectrum sensing is considered to be a significant technology enabling DSA. Although several spectrum sensing techniques have been proposed in the open literature, energy detection is widely used due to its low implementation complexity [4]. We discuss some of the spectrum sensing techniques along with energy detection below.

- In energy detection (ED) scheme the energy of the signal is detected in the frequency location and based on the threshold value we decide whether the signal is present or absent.
- Cyclostationary Feature Detection is a complex scheme to implement compared to ED and it is mostly used when we need to also classify the signal present based on

their modulation scheme.

- When secondary user has a priori knowledge of primary user signal, matched filter (MF) detection is applied. Detection by using matched filter needs less detection time compared to ED but primary user information is required.

These spectrum sensing techniques can be used in a non-cooperative manner but it is very challenging to get an accurate estimate using a single-sensor system under a practical fading environment. Various non-idealities such as shadowing, multipath and fluctuating noise variance can make it difficult to detect the primary user [5, 6]. Cooperative spectrum sensing can mitigate the effects of multipath and shadowing by utilizing the spatial and temporal diversity of a multiple radio network [7, 8]. In cooperative spectrum sensing, each sensor node collects the spectral data and transmits it to a fusion center (FC) for decision making. Figure ?? shows how a heterogeneous sensor network exploits the spatial diversity.

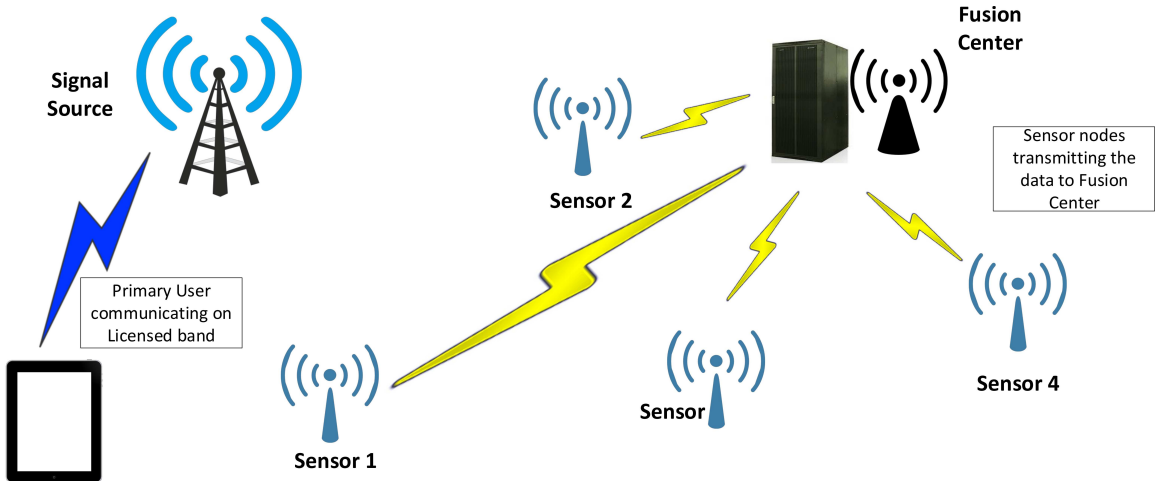


Figure 1.1: Heterogeneous sensor network employing cooperative spectrum sensing.  $RFFE_i$  and  $SR_i$  represents different front end and sampling rates for the SDR units.

We have also analyze the performance of Long Term Evolution for Railways (LTE-R) in a tunnel environment. In recent years, the use of trains have witnessed tremendous growth due to their increasing speeds, which has led to the demand for reliable wireless communication systems with these transportation systems. The development of a reliable wireless network for high speed trains is not a simple task and it is still an emerging technology. Global

System for Mobile Communication (GSM-R) [9], was a wireless communications standard designed for high speed trains, but it turned out not to be reliable enough and possess several limitations. Subsequently, LTE [10] proposed a promising solution for achieving broadband data rates in high speed trains that can overcome various GSM-R limitations [11, 12].

LTE-R is a high speed communication standard based on the existing LTE system architecture [12]. There has been several studies regarding the assessment of LTE-R as a viable choice for next generation high speed communications for railway applications [13, 14]. Most LTE systems operate at 1.8 GHz – 2.6 GHz bands, which possesses a high propagation loss and severe fading effects. Highly mobile trains inside tunnel environment makes the design of reliable communication links very challenging. To achieve reliable radio coverage inside tunnels, leaky feeder cables have been proposed [15]. With LCX, more uniform coverage can be achieved and installation is also comparatively simple. Each slot in the cable is equivalent to an antenna, which can transmit and receive signals. Figure ?? shows the LOS propagation environment inside a tunnel for a high speed train with velocity  $v$ .

## 1.2 State of the Art

The cooperative spectrum sensing testbed using normalized energy detection has been implemented and has been compared for both soft and hard data fusion scheme. Both soft data fusion and hard data fusion have been extensively studied [16–18], with several algorithms being implemented for each scheme. In a hard decision approach, each local decision statistic from sensor node is transmitted to an FC via overhead channels. The FC merges the sensing data and makes a global decision based on various algorithms such as majority rule, OR rule and AND rule [19]. For a soft decision scheme, each SU sends its local sensing data to the FC, which makes decision based on a global test statistic  $G$ . Soft decision combining improves the cooperative gain but it also possesses several limitations. With an infinite bandwidth, the real floating values can be transmitted to the FC, which can lead to a reliable decision mechanism. However, due to bandwidth constraint we have to quantize the data and this leads to error in the energy values. In hard decision combining, we can just transmit the decisions of the sensor nodes to the FC which can be binary values

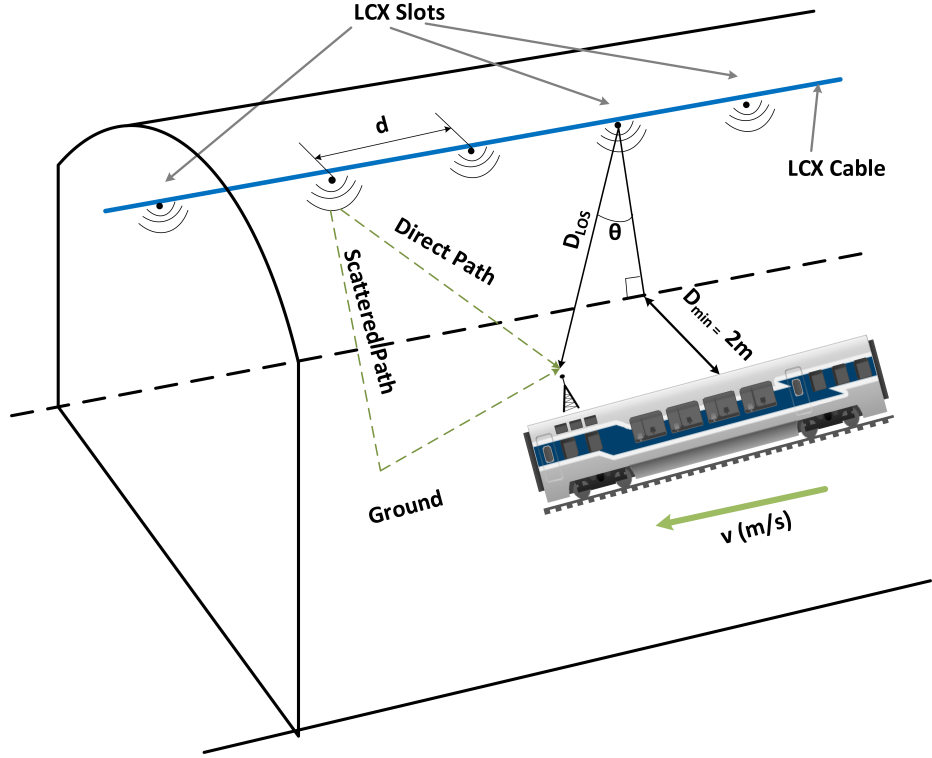


Figure 1.2: High speed train inside a tunnel for LTE-R.  $D_{LOS}$  is the distance between transmitter and receiver,  $d$  is the distance between the LCX cable transmission slots.

with 1 indicating that signal source is present and 0 indicating that a signal source is absent.

In open literature, most channel modeling have considered open areas with high speed trains [13, 14], while relatively little research has been conducted in tunnel environments. Due to various challenges presented by tunnel environments, it is important to derive a channel model for LTE-R involving high speed trains. In this paper, we analyze the effects of high Doppler shift and multipath due to tunnel environments. Experimental studies conducted inside tunnel environments have shown that the field amplitude distribution fits smoothly over a Rician distribution [20]. Several research efforts have been conducted on large-scale and small-scale fading of wideband communication systems inside tunnel environments. To the best of the authors knowledge, none of these studies have been conducted for LTE-R, which employs Orthogonal Frequency Division Multiplexing (OFDM) signals for data transmission inside tunnels. The large Doppler shifts caused by high speed

trains will potentially lead to ambiguity in extracting the carrier frequency, which can drastically increase the BER [21]. Therefore, it is important to study the effects of high Doppler shift and multipath fading for LTE-R communications in tunnel environments such that equalizers can be designed efficiently.

### 1.3 Thesis Contributions

This thesis will contribute the following to the cognitive radio communications and cellular wireless field:

- A cooperative spectrum sensing test-bed with normalized energy detection using both soft data fusion and hard data fusion implemented on available software defined radios.
- For soft data fusion, Maximum Normalized Energy (MNE) and Equal Gain Combination (EGC) algorithms are used. Hard data fusion is also implemented using majority rule, AND, and OR approaches. Both USRP N210s [22] and RTL-SDRs [23] are employed for the implementation of the heterogeneous sensor network.
- A performance assessment and simulation of LTE-R communications in a tunnel environment experiencing severe fading.
- Dynamic K-factor for a tunnel environment is derived using the classical two-ray propagation model [24] and is used to build Rician fading model for the tunnel.

### 1.4 Thesis Organization

This thesis will be organized into the following chapters: Chapter 2 provides background knowledge on heterogeneous cooperative spectrum sensing and focuses on heterogeneous networks, cooperative spectrum sensing and software-defined radios. Chapter 3 discusses LTE-R in detail and provides the necessary understanding of the LTE-R implementation in a tunnel environment. Leaky Coaxial Cable (LCX), channel impairments and two-ray propagation model is also discussed in detail. In chapter 4 and 5 implementation of heterogeneous cooperative spectrum sensing (CSS) test-bed and LTE-R performance

analysis in a tunnel is discussed. Chapter 6 presents the results of the implementation of heterogeneous CSS test-bed and LTE-R in a tunnel. Chapter 7 concludes this thesis, summarizing the accomplishments and outlines possible future work.

## Chapter 2

# Introduction to 5G and Key Technologies

The rapid advancement in the wireless communications shows the huge success in the wireless communication system. The advancement started with second generation (2G) system's debut in 1991 which were commercially launched on the GSM standard in Finland by Radiolinja. 2G systems were significantly more spectrally efficient compared to their predecessors and 2G also introduced the data services for mobile starting with SMS text messages, picture messages and multimedia messages (MMS). From 2G we migrated to 3G system which were first launched in 2001 and had fast mobile Internet access. 3G also introduced video calls and mobile TV and was able to provide information transfer speed of at least 2 Mbit/s. The 4G wireless systems were designed to be fully based on IP telephony where all the voice communications and multimedia sessions are delivered over Internet protocol (IP) networks [25]. 4G systems use orthogonal frequency division multiplexing (OFDM), multiple-input multiple-output (MIMO), and link adaptation technologies for a long term evolution (LTE) radio interface. 4G wireless networks can support data rates of up to 1 Gb/s for low mobility and up to 100 Mb/s for high mobility scenarios. The next evolution in wireless mobile communications is the fifth generation (5G) which is expected to be deployed by 2020.

Due to a sharp increase in number of wireless mobile devices and the shortage of the

wireless spectrum, researchers have started to investigate 5G wireless technologies. It is expected that the 5G network will achieve 1000 times the system capacity, 10 times the spectral efficiency, energy efficiency, data rate and 25 times the average cell throughput. This translates to a peak data rate of 10 Gb/s for low mobility and peak data rate of 1 Gb/s for high mobility scenarios. The table ?? below shows the comparison between 2G, 3G, 4G and 5G cellular communication system.

Table 2.1: Cellular Technologies Comparison between different generations of deployed digital cellular networks. Data rates, standard and implementation technology is compared for the 3G, 4G and 5G

<b>3G</b>	<b>4G</b>	<b>5G</b>
1990/2002	2000/2010	2010/2022
2 Mbps	200 Mbps – 1 Gbps (low mobility)	10 Gbps and higher (low mobility)
WCDMA, CDMA-2000	Unified Long Term Evolution (LTE) standard	In-progress

## 2.1 5G Cellular Architecture

The base station density is increasing drastically due to the huge spike in the use of heterogeneous networks to support massive exchange of information over the air. The heterogeneous networks are already standardized in 4G but the architecture is not natively designed to support them. The huge network densification requires major changes in the cellular architecture of 5G communication system. Wireless users mostly stay indoors for about 80% of the time, while only 20% of the mobile users stay outdoors [26]. The conventional cellular architecture consists of an outdoor base station in the middle of a cell communicating with mobile users irrespective of the user's location. Since the signal incur a large penetration loss since it has to go through buildings, thus restricting the data rates, spectral and energy efficiency of the wireless transmissions. The key idea behind 5G cellular communication is to separate the outdoor and indoor scenarios so that the penetration loss and shadowing caused by buildings can be avoided. This will be achieved by using distributed antenna system (DAS) and massive MIMO technology (also referred to as

"Large-Scale Antenna Systems") where spatially located antenna arrays with hundreds of antenna elements are deployed. Using large number of antenna arrays in base station renders the channels to the different devices quasi-orthogonal and very simple spatial multiplexing procedures quasi-optimal. The favorable action of the law of large numbers smoothens out frequency dependencies in the channel and thus leads to huge gains in the spectral efficiency [27]. The BSs deployed outdoors will be equipped with massive MIMO distributed around the cell and connected to the BS via optical fibers as a backbone network. The outdoor mobile users are normally equipped with very limited number of antenna elements, but the devices can form a virtual massive MIMO links to increase the capacity and spectral efficiency. The Figure 2.1 shows the proposed heterogeneous 5G cellular architecture by C. Weng, et.al [28].

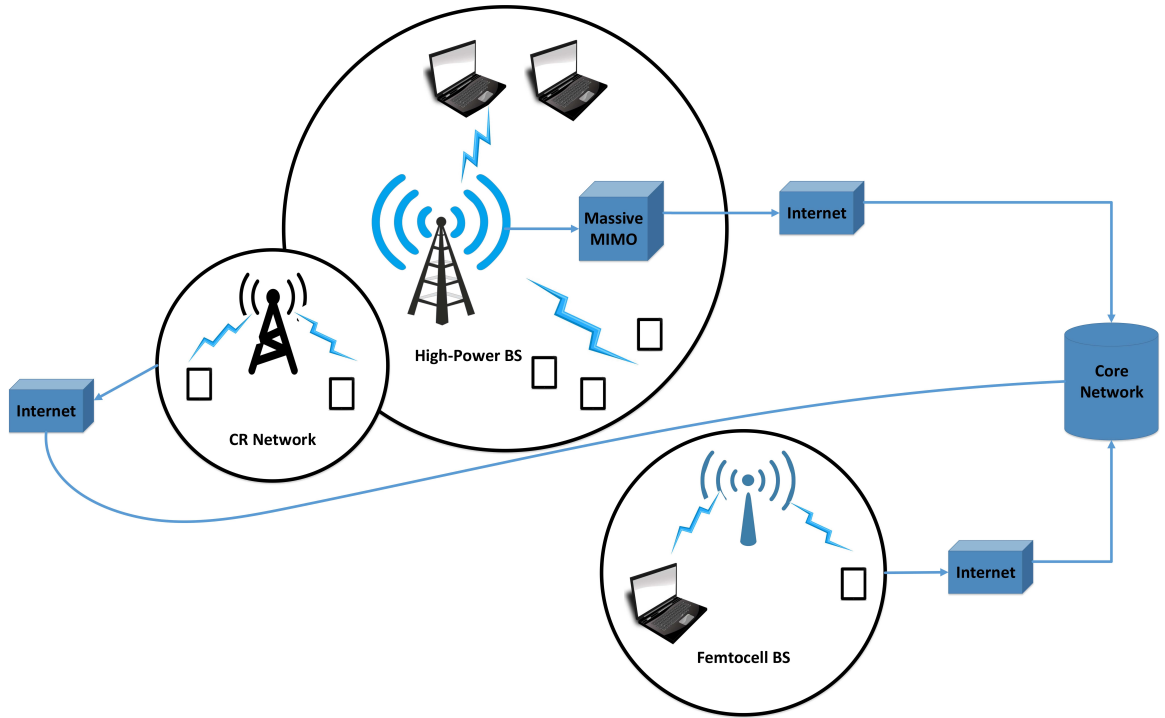


Figure 2.1: 5G Architecture

The proposed 5G cellular architecture consists of macrocells, microcells, small cells and relays. In this type of network, mobile users can be offloaded to nearby femto base stations instead of all competing for macro cells to increase the data rates per user. The massive MI-

MOs will be deployed outside of the buildings and will be connected to the wireless access points inside the building via cables for indoor users. The initial startup cost for the 5G infrastructure will be very high but it will vastly improve the cell throughput, spectral efficiency and data rate of the cellular system in the long run. By separating the cellular architecture into indoor and outdoor scenarios, with indoor users only requiring to communicate with indoor wireless access points many technologies can be utilized for short-range communications with massive data rates. The examples of short-range communications system include high speed Wi-Fi, ultra wideband (UWB) , mm-wave communications (3–300 GHz) [29] and visible light communications (VLC) (400–490 THz) [30]. The backbone networks of 5G will move from copper and fiber to mm-wave wireless connections enhancing cooperation and connectivity between base stations. It is worth noting that mm-Wave and light communication systems use higher frequencies not traditionally used for cellular technologies. Using mm-Wave frequencies currently saturated radio spectrum band from 700 MHz to 2.6 GHz can also be augmented for wireless communications. The 28 GHz and 60 GHz bands are currently available with spectrum allocations of over 1 GHz of band-width. Originally intended for Local Multipoint Distribution Service (LMDS) use in the late 1990's, these licensees could be used for mobile cellular as well as backhaul [31]. These sub tera-hertz frequency waves do not penetrate solid building walls very well and can readily be absorbed or scattered by gases, rain, and foliage. The path-loss at 60 GHz at 1m distance is around 68 dB and at 10 m distance path-loss is 88 dB. Therefore, it is hard to use these waves for outdoor and long distance applications. However, with large bandwidths available, mm-Wave and visible light communication technologies can greatly increase the transmission data rate for indoor scenarios. Besides using mm-Wave and VLC, dynamic spectrum access (DSA) can also be utilized to solve the spectrum scarcity problem. The important characteristics of DSA systems is their ability to exploit knowledge of their spectral environment to adapt and modify their operational parameters to efficiently access the spectrum [32]. The key promises of these systems are that they open up the possibility of highly flexible and efficient management and reuse of spectrum across all its dimensions. The cognitive radio [33], build on software-defined radio is the intelligent, adaptive and frequency agile wireless devices that will underlie most forms of future DSA systems. In this thesis, we have

implemented the cooperative spectrum sensing using software-defined radios which are utilizing the spatial gain to improve the accuracy of primary user detection. The primary user detection is very important factor in utilizing the spectrum efficiently so we don't interfere with the incumbent users. The heterogeneous networks has already been introduced in 4G LTE architecture but their use has been very limited and due to rapid densification of wireless devices 5G cellular architecture should be a heterogeneous one. In the following sections we will discuss the some key technologies which will drive the advancement of 5G cellular system.

## 2.2 Key Technologies of 5G System

To understand the engineering challenges facing 5G cellular communication, it is paramount to first identify its requirements. The following items are requirements in each key dimension, but it is important to note that all of these need to be satisfied simultaneously to achieve bounds set for 5G technology. Due to the rapid advancement in IoT devices different applications will place different requirements on the performance of the network. Applications with high data rate for e.g., streaming high-definition videos may have relaxed latency and quality of service (QoS) requirements compared to driverless cars or public safety applications, where latency QoS are paramount but lower data rates can be tolerated. Before we get into the key features of 5G cellular system, we first need to classify the impact of new technologies and their implications for 5G. These new technologies are classified leveraging the Henderson-Clark model and are as follows [?]:

- New changes are required at both the node and architectural level, for e.g. the introduction of codebooks and signaling support for a large number of antennas (Massive-MIMO).
- Complex changes in the design of network nodes are required, for e.g. introduction of new waveforms. These are the modifications required at the component level.
- The heterogeneous architecture of 4G system will act as a good benchmark for future 5G systems, but we need disruptive changes in the 5G system architecture.

- To achieve data rates in the order of tens of gigabits with much lower latency cannot be achieved by merely building on the current system architecture, we need to completely redesign the system at node and component level.

Some key features for the 5G wireless system which we think will be important in revolutionizing the cellular radios for the massively dense wireless devices in the future.

### 2.2.1 Massive MIMO

Massive (Very Large) multiple-input multiple-output MIMO Systems is a multiple antenna technology which is becoming ready for wireless communications and has been implemented for wireless broadband standards like LTE and Wi-fi. The key idea behind using large number of antennas is to create more possible signal paths and to achieve better performance in terms of data rate and link reliability via spatial multiplexing [34]. Figure 2.2 describes the implementation of massive MIMO technology using the patch antenna arrays communicating with several user equipments (UE). The implementation is proposed for the 5G system as the patch antenna arrays can be mounted on the walls of the buildings due to their thin size and can provide high-speed data rate coverage in outdoor environment also.

Massive-MIMO is the key technology for 5G cellular system and it has a clear distinction from the existing LTE/4G system through the use of a very large number of service antenna that can operate adaptively and in a fully coherent manner. It proposes utilizing a very high number of antennas to multiplex data signals for several UEs on each time-frequency resource, focusing the beam toward the intended directions while minimizing intra- and inter-cell interference. Using hundreds and thousands of antennas help in focusing the beam in a smaller regions of space, thus bringing huge improvements in throughput, gain and energy efficiency. This can particularly help in bringing large improvement when combined with simultaneous scheduling of a large number of UEs. Figure 2.3 shows the beamforming using  $N = 4, 8, 12$  and 16 antenna elements using linear dipole arrays. The antenna array gain for  $N = 4, 8, 12, 16$  is 9.23 dB, 12.3 dB, 14.1 dB and 16.15 dB respectively. By using hundred or thousands of antenna array element we can achieve a very high gain and throughput. Massive MIMO may require major architectural changes, particularly in the

## Massive MIMO Patch Antenna Array

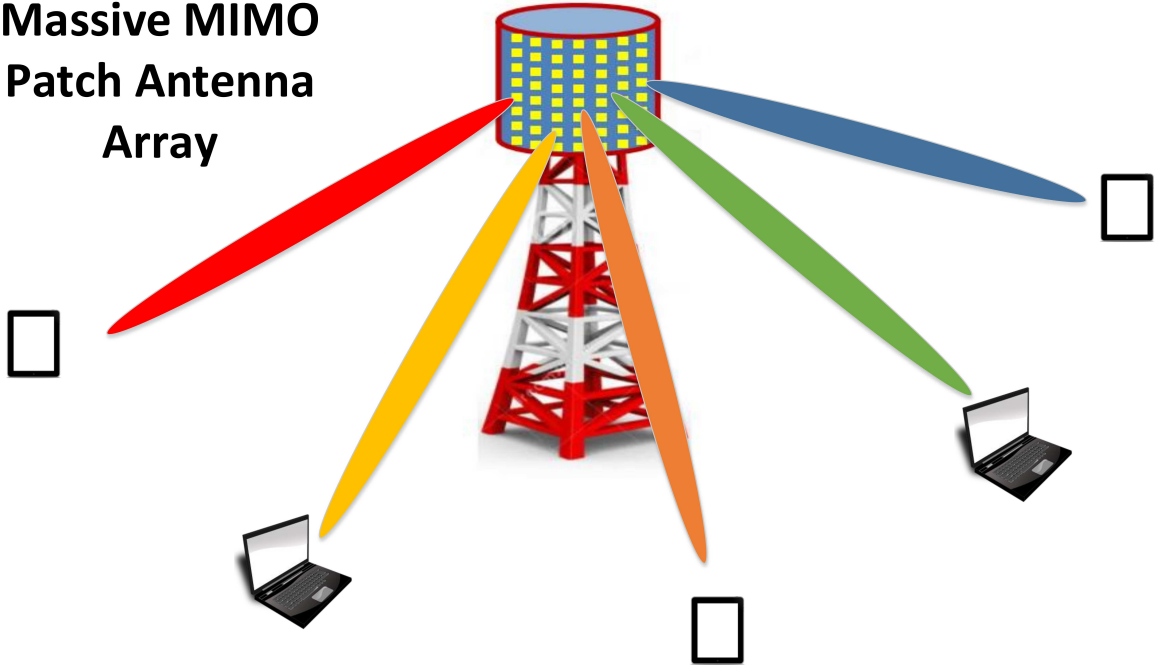


Figure 2.2: Massive-MIMO implementation using patch antenna arrays

design of macro base stations, and it may also lead to new types of deployments.

Using Massive-MIMO in 5G system will also lead to making extensive use of inexpensive low-power components, low latency and simplification of media access control (MAC) layer. Although with the arrival of massive-MIMO many traditional problems have become irrelevant, it opens up an entirely new areas research in 5G system. While a very promising technology, massive-MIMO still presents a number of research challenges which need to be addressed. Acquisition of channel state information (CSI) is critical and currently represents the main source of limitations. The mobility of users imposes a finite coherence interval during which channel knowledge must be acquired and utilized, and consequently there is a finite number of orthogonal pilot sequences that can be assigned to the devices [27]. There is still a lot of research which need to be conducted in massive-MIMO propagation, some experiments thus far have supported the hypothesis of channels being quasi-orthogonal. Synchronization is also very important issue for large number of antenna arrays with the need for reduced power consumption. These are some of the issues which need to be taken care of, for the next generation cellular system.

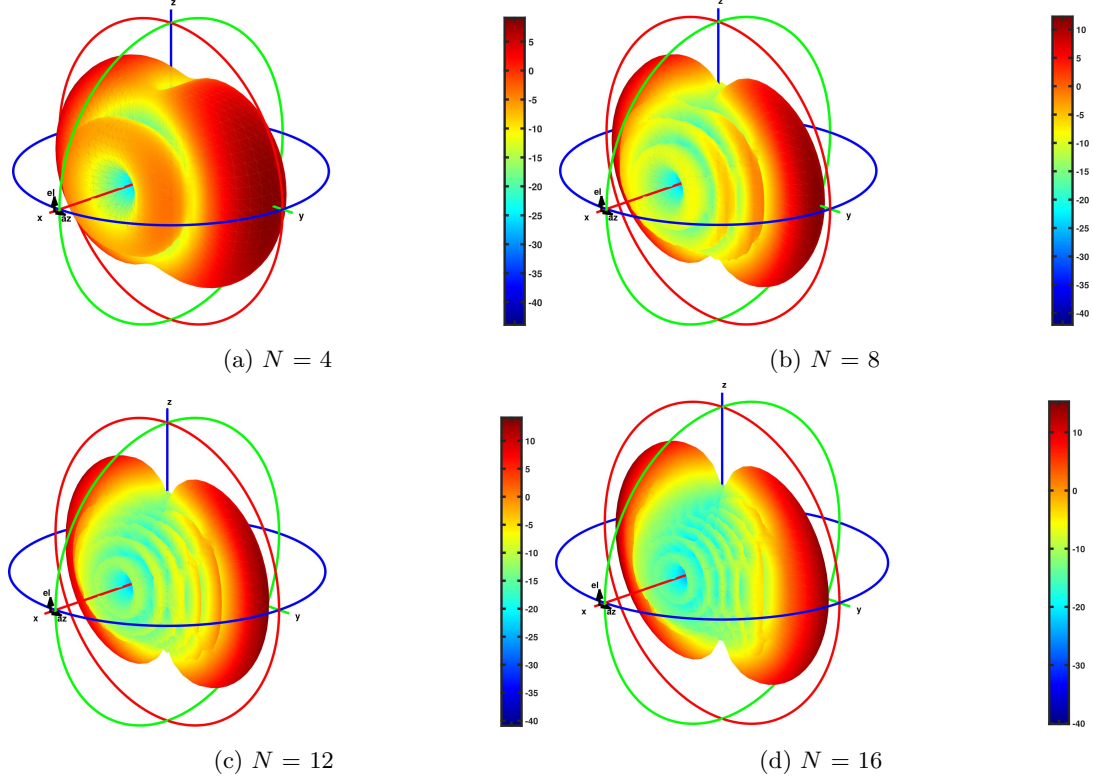


Figure 2.3: Beamforming for  $N=4$ , 8, 12 and 16 linear dipole antenna elements. As the number of antenna element increases we see a sharper beam confined in a smaller region. Massive-MIMO can utilize beamforming to increase spatial gain and spectral efficiency.

From above discussion, it can be concluded that implementation of massive-MIMO for 5G cellular system could represent an important breakthrough and major leap with respect to the current state-of-the-art in cellular technology. These modifications at system level needs to be justified for its massive infrastructure cost by solving the challenges currently faced by this key technology via simulations and test-bed experimentations.

### 2.2.2 Machine-to-Machine (M2M) Communication

Machine to machine (M2M) communication is a new paradigm proposed to be a key technology in 5G wireless systems that enables the ubiquitous connectivity between a set of devices with different network stack. Thus, the autonomous connection of devices facilitates the emergence of a wide range of intelligent M2M applications. M2M exhibits a strong po-

tential to improve human life in different fields such as e-Health, smart grids, smart cities, intelligent transportation and surveillance enabling internet of things (IoT) applications. A native inclusion of M2M communication in 5G involves satisfying three fundamentally different requirements associated with different classes of low data rates and power consumption services such as: enabling massive number of low-rate devices simultaneously, a minimal data rate in virtually all scenarios, even in worst fading environment and finally managing the above two requirements with a very low latency.

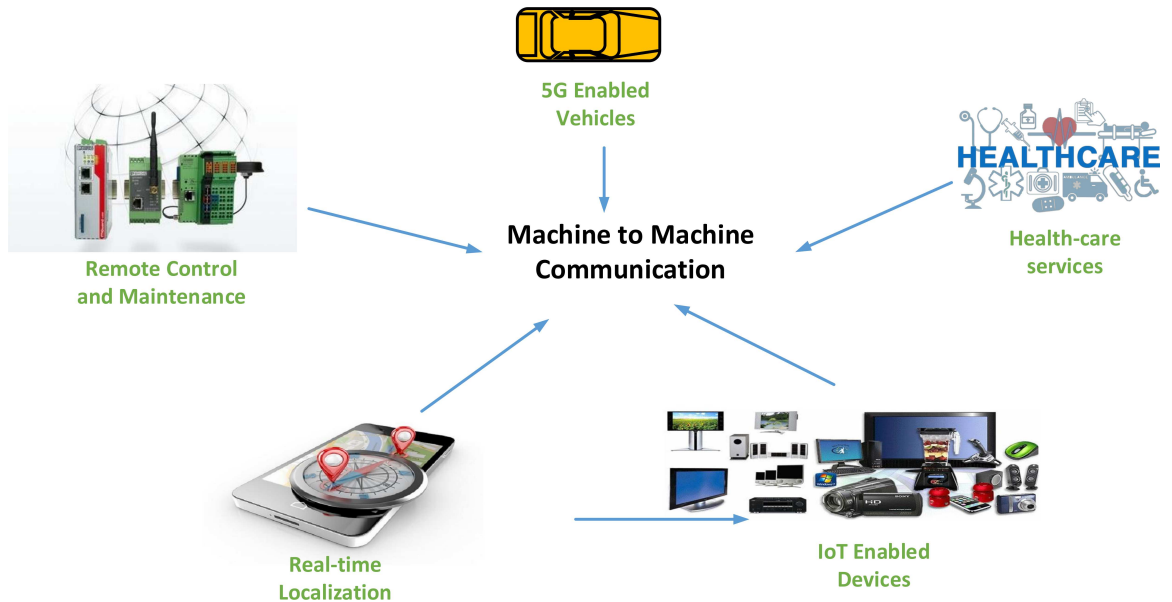


Figure 2.4: Machine-to-Machine communication paradigm in 5G Cellular System.

Implementing these requirements for 5G system, new communication paradigms needs to be developed at network and physical layer. Figure 2.4 shows the machine-to-machine communication and how it helps in integrating devices which can be used in health care, localization, vehicular communication, remote maintenance and consumer electronics. In the future standardization of the 5G networks, the M2M communication is recognized as one of the key technologies that will support the 5G architecture. As a consequence of this proliferation of M2M technology, large numbers of devices will produce huge amount of irregular data and significantly higher capacity of cellular networks will be needed, in terms of spectrum, power control as well as the number of devices serviced simultaneously.

For next generation 5G system, it would be common to have situations where devices will be in close proximity to each other and would like to wirelessly share data like videos, images, etc. or would like to interact for gaming, social networking. If these communication scenarios are handled by simply connecting through the network it can lead to various inefficiencies at various levels. The reason is that cellular networks were primarily designed to support mobile devices with a large amount of data to transmit, whereas most M2M communications are duty-cycling and delay-tolerant with small data packets between stationary terminals [35]. Thus, connecting a massive number of M2M devices directly with cellular networks will saturate uplink traffic easily [36]. In this context, non-cellular connections should serve as important supplement and extension to cellular networks. Some of the challenges of connecting the devices via cellular networks are:

- Multi-hopping is used to reach destination which otherwise requires fundamentally a single hop. This entails a multi-fold waste of signaling resources as well as higher latency.
- Huge amount of transmit power is consumed in uplink( fraction of a watt) and down-link( several watts) for data communication which can be easily achieved by milli-watts of power. This leads to unnecessary levels of battery drainage and interference to all other devices occupying the same signaling resources in near proximity.
- Propagation path-losses to the base stations are much stronger than direct link to the device, hence the corresponding spectral inefficiencies are also lower.

It is pretty evident that M2M has huge potential to handle single hop inter device communication more efficiently but these task could be offloaded to other radio access technologies such as Bluetooth, ultra-wide band (UWB) or Zigbee. The applications requiring a mixture of low-latency and high data rates for e.g. interaction between users via augmented reality could be more apt for 5G M2M communication system. In particular, machine-to-machine is as an important enabler for applications requiring low latency, especially in future network deployments utilizing baseband centralization and radio virtualization. There are still various research challenges which need to be taken care of before we can integrate this

technology in 5G cellular communication system. The devices for M2M communication need to be designed from both hardware and protocol perspective by providing the needed flexibility at both the PHY and MAC layers. Research needs to be conducted for possible extra overheads for control and channel estimation and also accessing of true net gains associated with M2M mode. And finally, accurate simulation and experimental test-beds needs to be designed for testing M2M communication.

### 2.2.3 Spectrum Regulation for 5G

Departing from technical issues, we now discuss the crucial interactions that 5G will encounter with spectrum policy and allocation by the federal communications commission (FCC). As already discussed in Section 2.1 the spectrum allocated for cellular technologies is already saturated in peak markets due to massive amounts of wireless services and networks. Figure 2.5 shows the pronounced scarcity in the the wireless cellular bands as seen in the FCC frequency allocation chart. Large amount of unused spectrum is available in the mm-Wave realm and can be used for high data rate applications. Due to different propagation characteristics for signals at low and sub-terahertz frequencies, future systems will need to integrate a broad range of frequencies. Frequencies on a lower spectrum can be used for wide coverage, mobility support, control signaling and high frequencies for high data rate applications in small cells. This requires a new approach to spectrum policy and allocation methods for 5G standardization.

Cognitive radio is a promising technology that can solve the spectrum shortage problem arising due to the rapid increase in wireless networks and mobile devices. Recent advancements in software-defined radio technology and edge computing have enhanced the cognitive radio network (CRN) capabilities and, along with some adjustments in its operation, will be a key technology for 5G heterogeneous network deployment. The CR network is an innovative software-defined radio technique considered to be one of the key technologies to improve the utilization of the congested radio spectrum [37]. Integrating CR technology into 5G system is motivated by the fact that a large portion of the radio spectrum is underutilized most of the time. For achieving data rates in order of gigabits per second, we need to make an efficient use of available spectrum which can be achieved by utilizing CRNs. In CR networks,

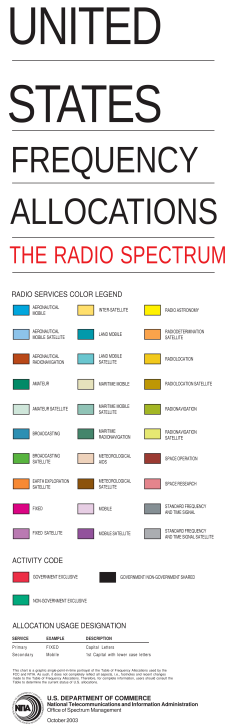


Figure 2.5: Machine-to-Machine communication paradigm in 5G Cellular System.

a secondary system can share spectrum bands with the incumbent primary system, either on an interference-free basis or on an interference-tolerant basis. The CR network should be aware of the surrounding radio environment and regulate its transmission accordingly. In interference-free CR networks, CR users are allowed to borrow spectrum resources only when licensed users do not use them. A key to enabling interference-free CR networks is figuring out how to detect the spectrum holes (white space) that spread out in wideband frequency spectrums and facilitate dynamic spectrum access (DSA) smoothly [38].

CR receivers should first monitor and allocate the unused spectrum via spectrum sensing (energy detection (ED), covariance absolute value (CAV) detection, etc.) or combining with geolocation databases and feed this information back to the central CR controller. A coordinating mechanism is required in multiple CR networks that try to access the same spectrum to prevent users colliding when accessing the matching spectrum holes. In interference-tolerant CR networks, CR users can share the spectrum resource with a licensed system while keeping the interference below a threshold. In comparison with interference-free CR

networks, interference-tolerant CR networks can achieve enhanced spectrum utilization by opportunistically sharing the radio spectrum resources with licensed users, as well as better spectral and energy efficiency. However, it has been shown that the performance of CR systems can be very sensitive to any slight change in user densities, interference threshold, and transmission behaviors of the licensed system. However, the spectral efficiency can be improved by either relaxing the interference threshold of the primary system or considering only the CR users who have short distances to the secondary BS (utilizing the spatial gain). Hybrid CR networks have been proposed in [39] for adoption in cellular networks to explore additional bands and expand the capacity. CR networks can only prove beneficial if the spectrum policies related to 5G are implemented in a robust manner.

### 2.3 5G using Millimeter Wave (mmWave)

The massive growth in wireless traffic has drawn an increased attention to the large amount of underutilized spectrum in the mm-Wave frequency bands as a possible solution for achieving gigabits of speed as promised for 5G implementation. Current spectrum for cellular radio (under 5 GHz) is congested and using CR network it can be made more efficient, but for 5G cellular system it is still better to go for bands above 10 GHz. A vast amount of largely unused spectrum is available and can be utilized for 5G. Wireless community has earlier ruled out mm-Wave for cellular usage due to the high penetration loss and its limited usage for short-range communications. And there was also the concern that rain and atmosphere make mm-Wave spectrum useless for mobile communications. The former problem is solved by dividing the cellular architecture into outdoor and indoor environment so that high-data rate applications can be implemented for direct line-of-sight (LOS) communication. As for latter when one considers the fact that todays cell sizes in urban environments are on the order of 200 m, it becomes clear that mm-wave cellular can overcome these issues [29]. In [40] recent results from channel measurement campaigns and development of advanced algorithms, a prototype is discussed in details which makes mm-Wave band a worthy candidate for next generation 5G cellular system.

Concerns regarding the propagation characteristics at higher frequencies such as higher

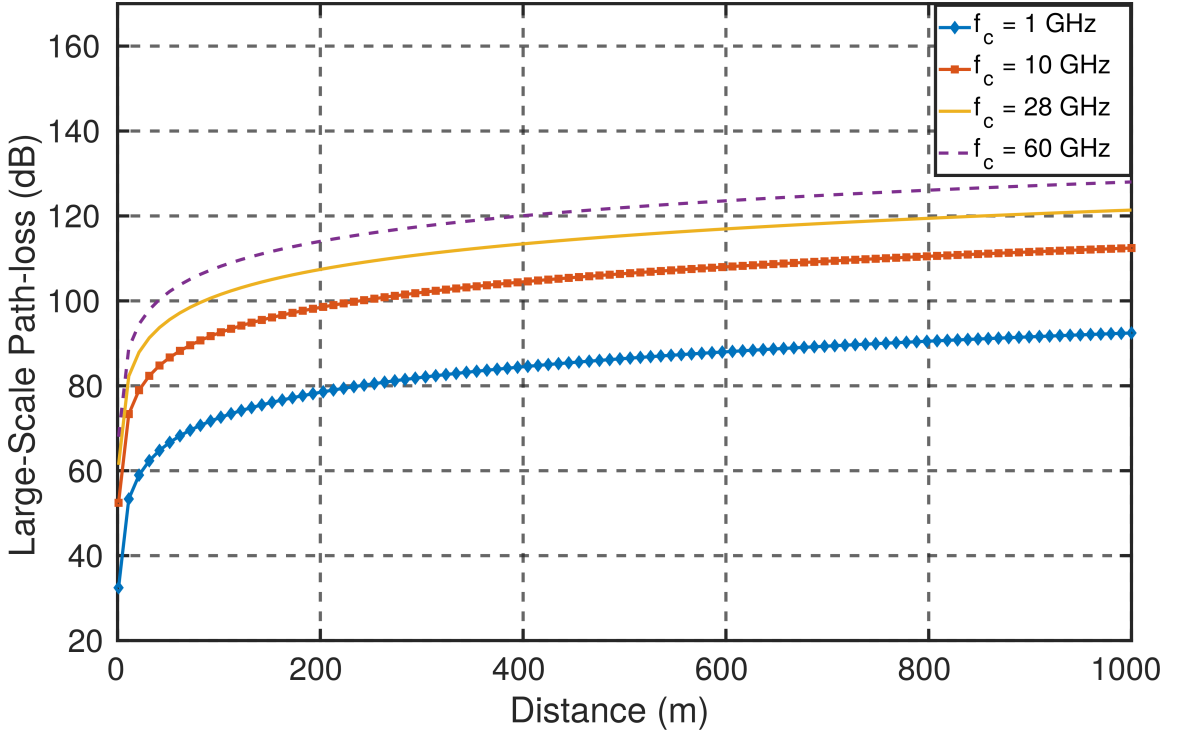


Figure 2.6: Large-scale propagation loss for  $f_c = 1 \text{ GHz}$ ,  $10 \text{ GHz}$ ,  $28 \text{ GHz}$  and  $60 \text{ GHz}$ .

penetration, precipitation, and foliage losses are legitimate even though the actual amounts of additional propagation losses vary depending on the material of the building, the strength of rain, or the thickness of foliage. Figure 2.6 shows the large-scale propagation loss for different frequencies and as we can see that as we go higher in frequencies, path-loss increases for an isotropic antenna. The plot also shows that after certain distance the propagation losses almost saturates and doesn't deteriorate as sharply as they do in first 10 meters. The most common misunderstanding, however, of the propagation characteristics at higher frequencies is that they always incur a much higher propagation loss even in free space compared to lower frequencies, and thus are not adequate for long-range communications. In [29] they have conducted laboratory measurements using a patch antenna at 3 GHz and an array antenna at 30 GHz of the same physical size within an anechoic chamber. And their results show same amount of propagation loss regardless of the operating frequency when an array antenna of the same physical aperture size is used at the 30 GHz receiving end. And additionally they also showed when array antennas are used at both transmitting

and receiving ends at 30 GHz, the measured receive power is 20 dB higher than that of the 3 GHz patch antenna case. To understand how the path-loss is same for 3 GHz and 30 GHz frequencies let's start with friis equation.

$$P_r = P_t + G_t + G_r + 20 \log \left( \frac{c}{4\pi df} \right) \quad (2.1)$$

where  $P_r$  is the received power in free space,  $P_t$  is the transmit power,  $G_t$ ,  $G_r$  are transmit and receive antenna gains, respectively,  $d$  is the distance between the transmitter and receiver in meters,  $f$  is the carrier frequency and  $c$  is the speed of light. From Eq.(2.1) it is pretty evident that received power is inversely proportional to the frequency squared for an ideal isotropic antenna. However, in reality antennas or an antenna arrays have gains of  $G_t$  and  $G_r$  greater than 1 and are typically employed at both ends. The most important factor for advocating mm-Wave is that antenna gains are proportional to the frequency squared given a fixed physical aperture size [41]. Given the same physical aperture size, therefore, transmit and receive antennas at higher frequencies, in fact, send and receive more energy through narrower directed beams, which is not commonly recognized. And since the physical size of antennas at mm-Wave frequencies is so small that it becomes practical to build hundreds and thousands of antennas elements to provide huge gains from spatial isolation and multiplexing for 5G cellular communication system.

## 2.4 Vehicular Communication Using 5G

With the development of mm-Wave and massive-MIMO, the spectral and energy efficiency for 5G wireless communications has been drastically improved. The development of driverless cars has posed some rigorous requirements for the safety of the passengers and pedestrians. For safety-critical applications the transmission delay needs to be less than 1 ms which is required for intelligent transportation systems (ITSs) and vehicular networks [42]. Considering the drawbacks of IEEE 802.11p networks, such as poor scalability, low capacity , and intermittent connectivity, the Long Term Evolution (LTE) mobile communication technologies were proposed to support vehicular applications [43]. Simulation and experiment results revealed that there is a trade-off between the proposed performance

metrics and system parameters, such as base station (BS) and vehicle densities, radio coverage, and the maximum number of hops in a path. When LTE communication technologies have been integrated into vehicular networks, the interference has cut down the performance of LTE vehicular networks. When vehicle density is high, the beaconing signals of vehicular safety applications may easily overload the serving eNodeB. To handle this issue, a significant amount of such signals should be distributed directly among vehicles, without going through the eNB. In LTE-Advanced (LTE-A), device-to-device (D2D) communication is considered to allow direct message delivery between terminals in proximity to lighten the load of eNB [44].

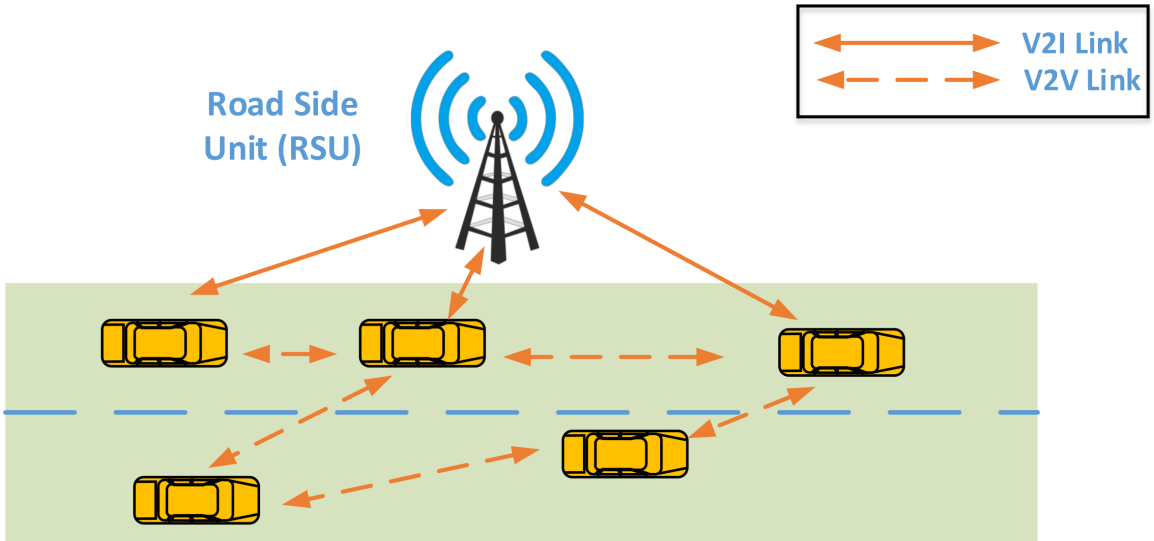


Figure 2.7: Vehicular communication using D2D 5G cellular communication technology.

Hence the infrastructure-aided D2D technologies can serve as a natural approach to enable reliable and efficient V2V communications without negatively affecting existing cellular systems. To meet the high performance requirements, such as low transmission delay and high throughput, a new architecture for 5G vehicular communication is required. Figure 2.7 describes the vehicular communication using D2D communication strategy where significant amount of computation is offloaded from road side units (RSU) to vehicles to avoid increase spectral and efficiency. The communication environment in V2V is quite different than in D2D due to high mobility (Doppler shift) of vehicles. Network connectivity play a important

role in V2V communication than D2D, compared with system throughput. These features can significantly affect D2D resource allocation strategies and system parameters, and thus should be modified for vehicular communication.

## 2.5 Summary

**Summary will go here for now use this demo msg** CR receivers should first monitor and allocate the unused spectrum via spectrum sensing (energy detection (ED), covariance absolute value (CAV) detection, etc.) or combining with geolocation databases and feed this information back to the central CR controller. A coordinating mechanism is required in multiple CR networks that try to access the same spectrum to prevent users colliding when accessing the matching spectrum holes. In interference-tolerant CR networks, CR users can share the spectrum resource with a licensed system while keeping the interference below a threshold. In comparison with interference-free CR networks, interference-tolerant CR networks can achieve enhanced spectrum utilization by opportunistically sharing the radio spectrum resources with licensed users, as well as better spectral and energy efficiency. However, it has been shown that the performance of CR systems can be very sensitive to any slight change in user densities, interference threshold, and transmission behaviors of the licensed system. However, the spectral efficiency can be improved by either relaxing the interference threshold of the primary system or considering only the CR users who have short distances to the secondary BS (utilizing the spatial gain). Hybrid CR networks have been proposed in [39] for adoption in cellular networks to explore additional bands and expand the capacity.

## Chapter 3

# Heterogeneous Cooperative Spectrum Sensing (CSS)

This chapter provides the background information needed to understand the chapters that follows. It examines the basic outlines of a heterogeneous networks and how cooperative spectrum sensing (CSS) can help in enhancing the accuracy of signal source estimation. The fusion center (FC) collects the data from the sensor node network and process it to make the reliable decision. Secondly, this chapter investigates various algorithms which can be used in heterogeneous network to estimate signal source. Finally, it also outlines the necessary hardware and software tools used in the implementation of heterogeneous CSS chapter.

### 3.1 Cognitive Radios

Cognitive radio (CR) [45] is a communication systems paradigm that focuses on employing highly agile, environmentally aware, intelligent wireless platforms in order to autonomously select and configure device operating parameters based on the prevailing radio and network environmental conditions [3]. In general the cognitive radio may be expected to look at parameters such as channel occupancy rate, available channels, bandwidth required for data transmission and the modulation types that may be used. It must also look at the regulatory requirements set by the Federal Communications Commission. In

some instances a knowledge of geography and this may alter what it may be allowed to do. Software-defined radios (SDR) are mainly responsible for making cognitive radios used in wireless communications system a reality. Software radios provide a vast untapped potential to personalize services, and they make the process of modifying the radio characteristics extremely simple.

The work is underway to determine the best possible methods of developing the cognitive radio communications system that can fulfill all its requirements. To facilitate the intelligent decision making capabilities in these cognitive radio systems, machine learning algorithms have been proposed in the literature [46–49] to automate the reconfiguration process. The Figure 3.1 describes the various building blocks of a cognitive radio system. The spectrum sensing is performed to estimate the spectrum holes in the band and after the analysis the decision strategy is prepared. The radio is configured with the new parameters based on the radio environment and the spectrum decision made.

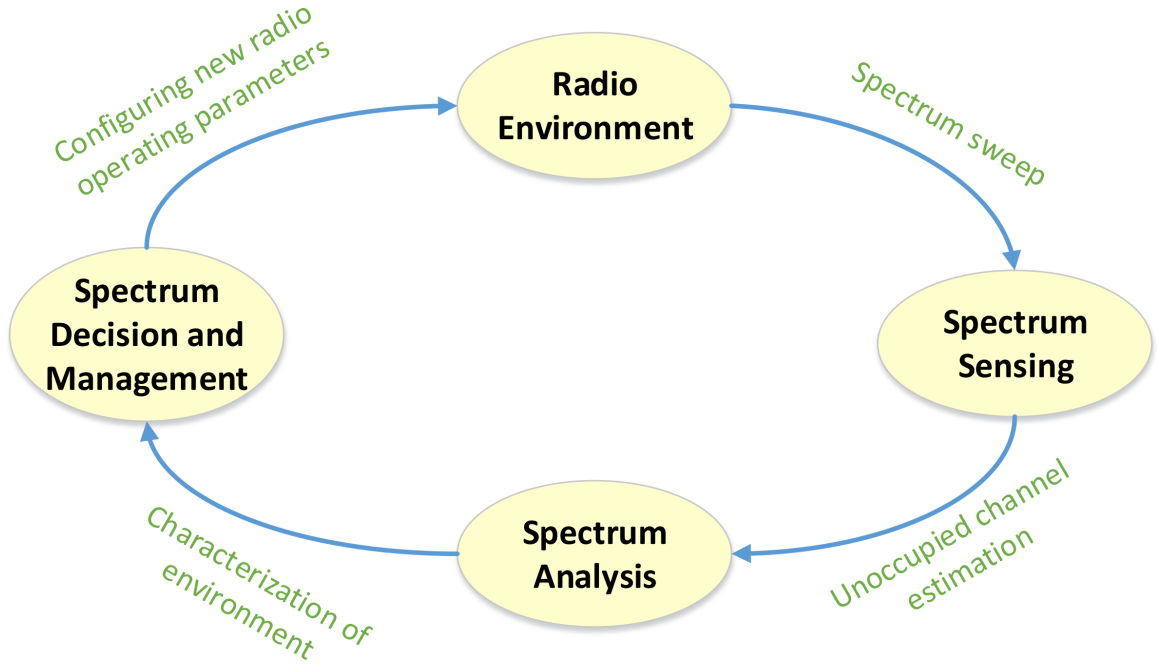


Figure 3.1: The block diagram explaining the basic parts of Cognitive Radio system. The operating parameters are configured based on the characterization of the wireless environment.

### 3.2 CSS in Heterogeneous Networks

In Heterogeneous CR network, each radio is equipped with different numbers of antennas, sampling rates and RF characteristics. In addition, each sensor node may experience distinct channel fading and suffer from different noise levels due to their respective locations and device performances, such as amplifier and ADC. As a result, each node may have different sensing capabilities and reliability values. This is a universal and fundamental characteristic of a heterogeneous CR network which requires robust algorithms to achieve high accuracy in signal source detection for estimating the presence of a primary user [50]. In this thesis, we investigate the cooperative spectrum sensing in heterogeneous networks with a centralized FC, a transmitter acting as a signal source and four sensor nodes. As explained earlier we are using energy detection as one of the spectrum sensing technique since it possesses a very low implementation complexity [4]. The energy detection scheme detects the presence or absence of a signal source based on its intercepted energy signature. If the energy of the signal is higher than a certain threshold, this indicates that the channel is occupied. The ED can be modeled by the equation:

$$y(n) = \begin{cases} w(n), & \mathbf{H}_0 \\ s(n) + w(n), & \mathbf{H}_1 \end{cases} \quad (3.1)$$

where  $y(n)$  represents the received signal,  $s(n)$  represents the signal source PU, and  $w(n)$  is the white Gaussian noise  $w(n) \sim N(0, \sigma_n^2)$ .  $\mathbf{H}_0$  describes the hypothesis when there is no signal present, while the hypothesis  $\mathbf{H}_1$  is the presence of signal.

The decision whether the signal is present or absent is decided by evaluating a local test statistic  $L$  to see whether it is above or below certain fixed threshold  $\tau$ . The local test statistic  $L$ , which is the complex-magnitude squared of the FFT samples, is compared with  $\tau$  using equation:

$$L = \sum_{n=1}^M |y(n)|^2 = \begin{cases} < \tau, & \mathbf{H}_0 \\ > \tau, & \mathbf{H}_1 \end{cases} \quad (3.2)$$

where  $|y(n)|^2$  is the energy of a specific FFT bin and  $n=1,2,3\dots M$  are the number of samples received.

The probability of false alarm  $P_{fa}$  and probability of detection  $P_d$  are given by:

$$P_f = Q\left(\frac{\tau - M(2\sigma_n^2)}{\sqrt{M(2\sigma_n^2)}}\right), \quad (3.3)$$

$$P_d = Q\left(\frac{\tau - M(2\sigma_n^2)(1 + \gamma)}{\sqrt{M(1 + 2\gamma)(2\sigma_n^2)}}\right). \quad (3.4)$$

In cooperative spectrum sensing, each sensor node transmits the local sensing data to the fusion center for signal source detection. The local sensing data has to be quantized, thus yielding quantization errors. To minimize the quantization error in local test statistic  $L$  and to reduce the effect of noise variance, the energy of the received signal  $y(n)$  is normalized [50].

The local test statistic  $L$  for the  $r^{th}$  sensor node is given as:

$$L_r = \frac{1}{M_r \sigma_{n,r}^2} \sum_{r=1}^{M_r} |y(n)|^2 \quad (3.5)$$

where  $M_r$  is the number of samples used to estimate the power of the signal source in the node,  $\sigma_{n,r}$  is the noise power variance.

In Eq (3.1)  $s(n)$  is considered as a deterministic signal and  $w(n)$  is a Gaussian random variable with a variance of  $\sigma_n^2$ . Based on CLT,  $L_r$  will have a following distribution [7]:

$$L_r = \begin{cases} N(1, \frac{1}{M_r}), & \mathbf{H}_0 \\ N(\gamma_r + 1, \frac{1 + 2\gamma_r}{M_r}), & \mathbf{H}_1 \end{cases} \quad (3.6)$$

where  $\gamma_r$  is the received SNR of the  $r^{th}$  SU. The local decision statistic  $L_r$  is quantized before transmission due to the bandwidth constraint, and this can lead to quantization errors. The values of  $L_r$  received by FC can be modeled as:

$$\beta_r = L_r + w_{q,r}, \quad (3.7)$$

where  $\beta_r$  is the decision statistic received by the FC and  $w_q$  is the noise added to the signal due to fading and quantization error. In [51], the  $w_q$  is modeled as a Gaussian noise with zero mean and  $\sigma_q^2$  variance.

### 3.3 Software Defined Radios

We have already explained about the cooperative spectrum sensing in heterogeneous networks, now in this section we will look at the platform for testing the CSS algorithms. The platform which we use is a new hardware frontier called Software-Defined Radio (SDR) and is discussed in details.

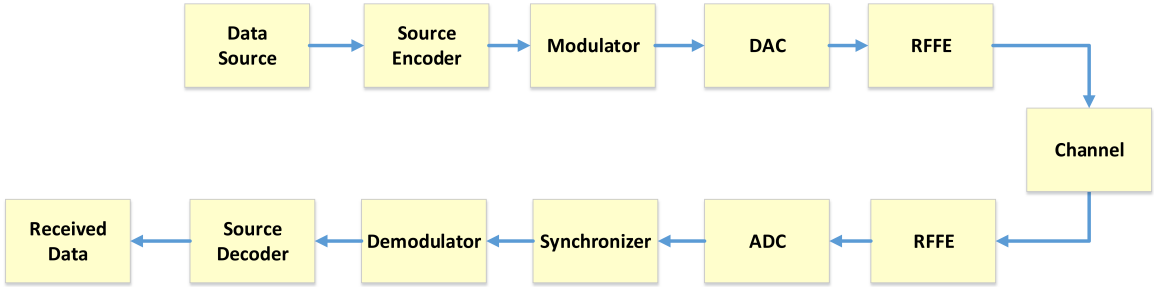


Figure 3.2: Software defined radio pushes all the adaptive elements and data manipulation operation into software. The goal of SDR is to provide or define all of the radio operation in software.

There has been a huge shift in the definition of a Software-Defined Radio and it has a lot to do with the question of where the hardware ends and software begins. Dr. J. Mitola III coined the Software Defined Radio which he described as a of digital signal processing (DSP) primitives, a meta-level system for combining the primitives into communication system (Tx, channel model, Rx, etc.), functions and a set of target processors on which the software radio is hosted for real-time communications [52]. Dr. J. Mitola explains in the thesis how software provides the flexibility which using hardware alone can never be achieved. And as time progresses SDR would become more dominant and close to ideal Cognitive Radio system.

The SDR technology existed since the 1970s but the key milestone in the advancement of SDR technology took place in early 1990s with the U.S. military initiative called SpeakEasy I/II. The SpeakEasy project was implemented to use programmable processing to emulate more than ten existing military radios, operating in frequency bands between 2 MHz and 2 GHz [53]. With SpeakEasy the operator could talk to ten radios operating under different

standards with any hardware modifications. With all these features, unfortunately there were some shortcomings which left much to be desired. The device was large enough to fit on the back of a pickup truck [53] which is good for ground station but not if the mobility is an important factor. And in 1992 the field programmable gate arrays (FPGA) were not computationally efficient, hence required large time to change their operating characteristics. The two software-defined radios we used in the thesis are Universal Software Radio Peripheral (USRP N210) and RTL-SDR R2832U. In the subsequent subsections we discuss the two SDRs in detail.

### 3.3.1 USRP N210 and RTL-SDR

The Universal Software Radio Peripheral (USRP) N210 has a very different RF characteristics compared to RTL-SDR hence modeling an ideal heterogeneous network. The USRP N210 provides a very high bandwidth, dynamic range processing capability. The product architecture includes a Xilinx Spartan 3A-DSP 3400 FPGA [54], 100 MS/s dual ADC, 400 MS/s dual DAC and gigabit ethernet connectivity to stream data to and from host processors. A modular design allows the USRP N210 to operate from DC to 6 GHz, while an expansion port allows multiple USRP N210 series devices to be synchronized and used in a MIMO configuration. An optional GPSDO module can also be used to discipline the USRP N210 reference clock to within 0.01 ppm of the worldwide GPS standard. The USRP N210 can stream up to 50 MS/s to and from host applications. Users can implement custom functions in the FPGA fabric, or in the on-board 32-bit RISC softcore. The USRP N210 provides a larger FPGA than the USRP N200 for applications demanding additional logic, memory and DSP resources. The FPGA also offers the potential to process up to 100 MS/s in both the transmit and receive directions. The FPGA firmware can be reloaded through the Gigabit Ethernet interface [22].

RTL-SDR is a very cheap software defined radio that uses a DVB-T TV tuner dongle based on the RTL2832U chipset. With the combined efforts of Antti Palosaari, Eric Fry and Osmocom it was found that the signal I/Q data could be accessed directly, which allowed the DVB-T TV tuner to be converted into a wideband software defined radio via a new software driver. Essentially, this means that a cheap \$20 TV tuner USB dongle with

the RTL2832U chip can be used as a computer based radio scanner. This sort of scanner capability would have cost hundreds or even thousands of dollars just a few years ago. The RTL-SDR is also often referred to as RTL2832U, DVB-T SDR, RTL dongle or the \$20 Software Defined Radio.

### 3.3.2 GNU Radio and Software-Defined Radio

We have used GNU Radio [55] and MATLAB software in the thesis to implement the cooperative spectrum sensing for hard decision and soft decision schemes. GNU Radio is an open source development toolkit that provides re-configurable signal processing blocks to implement and test out software-defined radios and signal processing systems. GNU Radio allows for SDR developers to develop unique signal processing blocks and SDR systems. GNU Radio was started in 2001, originally forked from the SpectrumWare project developed at the Massachusetts Institute of Technology. Since 2001, the code base has undergone massive changes, containing almost no code from the original SpectrumWare project [56]. Physically the code consist of three languages Python, C++, and SWIG. Python provides the overarching control of the system or program, while C++ provides the actual signal processing blocks and mathematics. SWIG is a wrapper for C++ which allows Python to dynamically wrap around C++ and control or compile with it. A diagram below better illustrates this architecture. It is also important to mention that there as significant paradigm shifts in the community, pushing more and more code to Python rather than C++, due to its easier programming syntax and structure [57].

The GNU Radio software provides the framework and tools to build and run software radio or just general signal-processing applications. The GNU Radio applications themselves are generally known as "flowgraphs", which are a series of signal processing blocks connected together, thus describing a data flow. GNU Radio provides a very structured framework of flow design. Data processing segments are extremely self contained to minimize error propagation during system debugging. Since the software is open-source full access to all code is provide, giving low-level access to all operation within GNU Radio. Much of the actions have been abstracted to the limited knowledge of the lower layers, but if specific actions are required for an application then serious depth or knowledge is needed about the

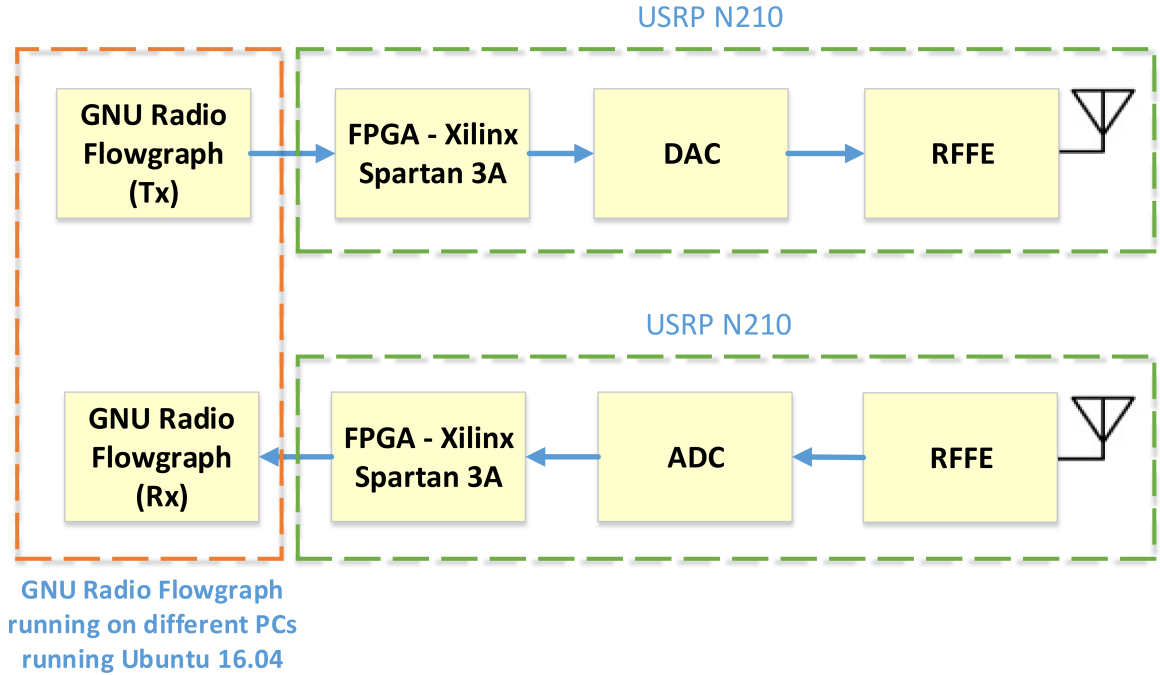


Figure 3.3: GNURadio and Software-Defined Radio

overall projects structure, which is quite overloading.

### 3.3.3 MATLAB

MATLAB [58] is an extremely well known engineering, mathematical, biological, and financial software suite. MATLAB provide massive data leverage and advanced communication system models and algorithm for significant data processing.

## 3.4 Summary

This chapter outlined and examined the topics of jamming and anti-jamming techniques, and provided a foundation in communication system theory and advanced equalizer design. Secondly it setup an understanding of Software-Defined Radio, the power of such an architecture, and examples of implementations and existing software for future designs. Next, this thesis will consider a new anti-jamming technique and design an implementation of such a system. After the implementation is investigated, the result of specific experiments

on such an implementation will be analyzed.

## Chapter 4

# Long Term Evolution for Railways (LTE-R)

This chapter provides background information on LTE proposed for high-speed railway communication system. It outlines the architecture for LTE-R leveraging the existing LTE network for high speed railway networks. For uniform coverage inside a tunnel environment, leaky coaxial cables (LCX) has been proposed for efficient communication. We explain LCX cables in details in the following chapter especially for tunnel environment. The severe channel impairments inside a tunnel are also discussed with special attention to high Doppler shift cause due to high velocities of trains and harsh multipath fading environment. Finally, the proposed two-ray propagation channel model is discussed and dynamic K-factor is derived.

### 4.1 LTE-R Communication System

In recent years, the use of trains have witnessed tremendous growth due to their increasing speeds, which has led to the demand for reliable wireless communication systems with these transportation systems. The development of a reliable wireless network for high speed trains is not a simple task and it is still an emerging technology. Global System for Mobile Communication (GSM-R) [9], was a wireless communications standard designed for

high speed trains, but it turned out not to be reliable enough and possess several limitations. The data rate of voice services which can reach up to 9.6 kbps, which can't meet the increasing demands of high-rate data transmission in railways communication. The limited data rate and quality of service (QoS) is not enough to support cellular communication for current generation. These reasons have made the evolution of high speed railway communication more and more urgent. Subsequently, LTE [10] proposed a promising solution for achieving broadband data rates, flexible bandwidth allocation and high spectral efficiency in high speed trains that can overcome various GSM-R limitations [11, 12].

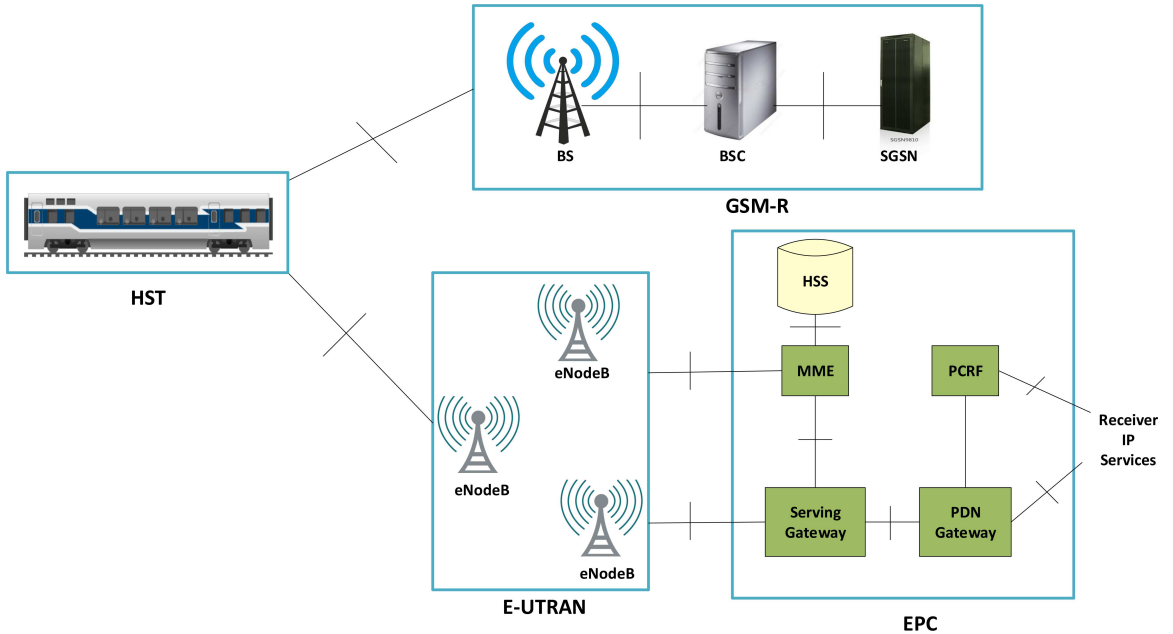


Figure 4.1: Proposed LTE-R Architecture for next generation High-speed Railways consisting of EPA and E-UTRAN.

LTE-R is a high speed communication standard based on the existing LTE system architecture [12]. There has been several studies regarding the assessment of LTE-R as a viable choice for next generation high speed communications for railway applications in [5, 6]. Conventional LTE includes a core network of evolved packet core (EPC) and a radio access network of Evolved Universal Terrestrial Radio Access Network (E-UTRAN). The Internet protocol (IP)-based EPC supports seamless handovers for both voice and data to cell towers, and each E-UTRAN cell will support high data and voice

capacity by high-speed packet access (HSPA). As a candidate for the next-generation communication system of HSR, LTE-R inherits all the important features of LTE and provides an extra radio access system to exchange wireless signals with onboard units (OBUs) and to match HST-specific needs. Figure 4.1 shows the proposed architecture of LTE-R according to [10], and it shows that the core network of LTE-R is backward compatible with GSM-R. The network architecture of LTE-R is similar to that of LTE/SAE with Evolved Universal Terrestrial Radio Access Network (E-UTRAN) being the access network structure of LTE-R. There is evolved-Node B (eNodeB) that communicates directly with UEs like base transceiver station (BTS) in GSM network. It performs the transmission and reception of data packets using orthogonal frequency division multiplexing access (OFDM) for downlink and single carrier frequency division multiple access (SC-FDMA) for uplink at PHY layer. At the same time, as without base-station controller (BSC), it also has functions of radio resource control and wireless mobility management. The eNodeBs can be connected to network router directly without more intermediate control nodes, such as the BSC in GSM-R [59]. The core network of LTE-R is the Evolved Packet Core (EPC). The significant difference between EPC and the core network of GSM-R is that the EPC is an all-IP mobile core network.

Table 4.1: Comparison of system parameters between GSM-R , LTE and LTE-R.

System Parameters	GSM-R	LTE	LTE-R
Frequency	Uplink: 876–880 MHz downlink: 921–925 MHz	800, 1800, 2600 MHz	450, 800, 1400, 1800 MHz
Capacity	0.2 MHz	1.4-20 MHz	1.4-20 MHz
Modulation	GMSK	QPSK/16-QAM/64-QAM	QPSK/16-QAM
MIMO	No	2x2, 4x4	2x2
Cell Range	8 Km	1-5 Km	4-12 Km
Data Rates (DL/UL)	172/172 Kbps	100/50 Mbps	50/10 Mbps

Conventional LTE networks are different compared to LTE-R in many ways such as architecture, system parameters, network layout, services and quality of service (QoS).

Table 4.1 summarizes the LTE-R parameters and describe the differences between LTE, GSM-R and LTE-R. Since the LTE-R environment has very severe fading and high Doppler shift, it is configured for QoS rather than higher data rates. Therefore, QPSK modulation is used for most number of subcarriers and the number of packet re-transmission must be kept low and achieved with user datagram protocol (UDP).

## 4.2 Leaky Coaxial Cable for LTE-R

Leaky Coaxial Cable (LCX) [60] is an antenna technology designed to deliver radio services in tunnel environment. It consists of small periodic slots to allow radio frequency (RF) signals to escape which act as extended antenna elements. LCX cables were invented to provide the uniform signal coverage in underground mine where radio coverage was very limited due to the geography of the mines. Recently, leaky coaxial cables have been widely used in the field of railway communication especially in tunnels. Leaky feeders are constructed from coaxial cable where the outer shield has a series of holes with different shapes and different distances among them. The coaxial cable is usually about hundreds of metres long and can be fixed through a building or a tunnel offering radio radiation in a way that would require many individual omni-directional antennae. So far, they have been only used to supplement the direct wireless communication system between a BS and trains, mostly transmitting voice signals. Nowadays, they are being used as an alternative solution to distributed antenna systems in indoor environments like commercial buildings [61, 62] and university buildings, high speed trains, cars, etc. The LCX radio system is almost noise free and has enough bandwidth to support multiple RF signals carrying voice and data simultaneously. Figure ?? shows the conventional leaky coaxial cable along x-axis with periodic radiating slots and wave propagation along z-axis. Generally, it consists of three parts: inner conductor, dielectric material and outer conductor. LCX has a dual functionality i.e. they can transmit and receive RF signals using their slots. The frequency range for a leaky cable is given by [63]:

$$\frac{c}{\sqrt{\varepsilon_r - 1)d}} \geq f \leq \frac{c}{\sqrt{\varepsilon_r + 1)d}} \quad (4.1)$$

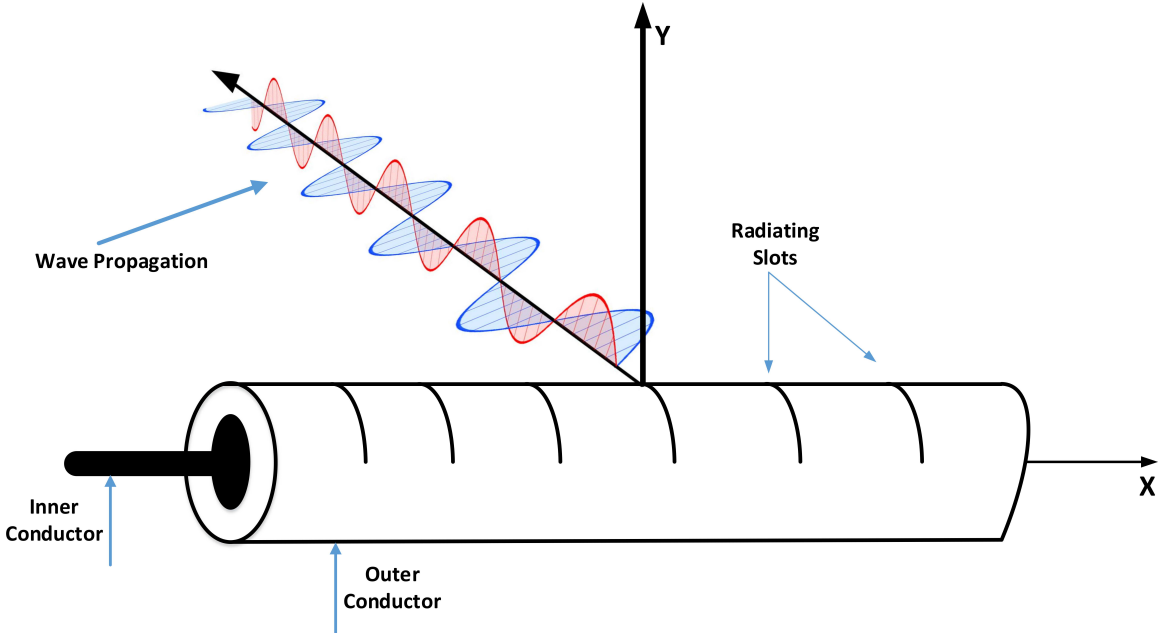


Figure 4.2: Leaky Coaxial Cable

A radio system based on LCX has been deployed in Japan for high speed railways "Series N700" [64] to connect the train to ground network. Wi-Fi access points are chosen for in-train communications with peak data rates of 2 Mbps for uplink and downlink. Although current technologies can provide wireless communication services in HSTs, the capacity of communication system is very low (1–4 Mbps). These data rates are insufficient for next generation wireless communication system where the peak data rates of 0.5 – 5 Gbps are expected. LTE-R communication system can be implemented for achieving high data rates but it cannot be achieved by using conventional cellular system. The penetration loss due to tunnel walls is very high and secondly, the fast moving trains causes large Doppler shifts leading to poor connectivity due to retransmissions. Hence, leaky coaxial cable is the best candidate for achieving extensive internet access inside a tunnel environment for high speed railways.

## 4.3 Channel Impairments Inside a Tunnel

The tunnel environment is affected by multipath and diffraction effects due to multiple reflections from the tunnel walls, which leads to a substantial fading environment. By deploying LCX cables, we can eliminate the large penetration loss due to tunnel walls. However, small-scale fading can still cause a large amount of errors and decrease the QoS for the communication link. High velocity trains experience very high Doppler shifts and a fast fading channel. These problems can lead to significant BER degradation of the LTE system. The frequency shifts caused by the Doppler phenomenon can lead to shifts in the sub-carrier frequencies for OFDM, which leads to synchronization errors. The maximum Doppler shifts for a train traveling at 500 km/h is 2.314 kHz for a 5 GHz carrier frequency. This large Doppler shift can also lead to significant drops in the quality of wireless signals and increase the bit error rate. Thus, to develop an efficient and reliable communication link inside tunnels, we need to properly model this channel impairment and build our proposed channel model by taking into account these tunnel phenomena. These impairments are described in detail in the following subsections.

### 4.3.1 Multipath Fading

The following time-varying multipath channel impulse response considers the effects of Doppler shift and scattering [65]:

$$h(\tau, t) = \sum_{k=0}^L h_k(t) e^{-j2\pi f_c \tau_k(t)} \delta[\tau - \tau_k(t)], \quad (4.2)$$

where  $\tau$  is the path delay,  $t$  is time in seconds,  $\delta[\tau - \tau_k(t)]$  is the impulse response,  $f_c$  is the carrier frequency,  $h_k(t)$  is the envelope of the time-varying channel and consists of both large and small-scale fading components. Since the structure of LCX is almost the same as a leaky waveguide, the large scale fading of channel can be modeled linearly [66]. There is also no signal shadowing and the line-of-sight (LOS) signal component is always present along the tunnel. This type of channel fading can be best described by a Ricean fading

model. The probability density function  $p(\alpha)$  of a Rician fading model is given by [67]:

$$p(\alpha) = \frac{2\alpha(1+K)}{\Omega} I_0\left(2\alpha\sqrt{\frac{K+K^2}{\Omega}}\right) e^{-\frac{-K-\alpha^2(1+K)}{\Omega}}, \quad (4.3)$$

where  $K$  is the Rician factor and  $\alpha$  is the complex amplitude of the channel response function that has a unity second moment, *i.e.*,  $\Omega \equiv E[\alpha^2] = 1$ .

### 4.3.2 Doppler Shift

The 3GPP channel model [68] is used for its Doppler shift profile in high speed railway environment. The measurements obtained for the Doppler frequency shift are implemented for two scenarios. The first scenario is for an open space while the second scenario is for high speed trains. Doppler shift is not taken into consideration. There exists a third scenario for tunnels using multiple antennas. Since the slots of LCX can be modeled as multiple antenna system, we use this Doppler shift profile for our proposed channel. The Doppler shift variation  $f_s(t)$  is described by:

$$f_s(t) = f_d \cos \theta(t), \quad (4.4)$$

where  $f_d$  is the maximum Doppler shift,  $\theta$  is the elevation angle and  $\cos \theta(t)$  is given by:

$$\cos \theta(t) = \begin{cases} \frac{D_s/2 - vt}{\sqrt{D_{\min}^2 + ((D_s/2) - vt)^2}}, & 0 \leq t \leq \frac{D_s}{v} \\ \frac{-1.5D_s + vt}{\sqrt{D_{\min}^2 + ((-1.5D_s) - vt)^2}}, & \frac{D_s}{v} \leq t \leq \frac{2D_s}{v} \end{cases} \quad (4.5)$$

where  $D_s/2$  is the initial distance of the train from base-station, and  $D_{\min}$  is base-station (BS)-Railway track distance, both in meters;  $v$  is the velocity of the train in m/s,  $t$  is time in seconds.

Figure ?? shows the Doppler spectrum for  $f_c = 5$  GHz and  $v = 300$  Km/h, 400 Km/h and 500 Km/h, and as we can see in the figure the maximum Doppler shift range is from -2.314 kHz to +2.314 kHz. These range of Doppler shift values can lead to very high bit-error rate and poor connectivity in communication system. In the following section we discuss

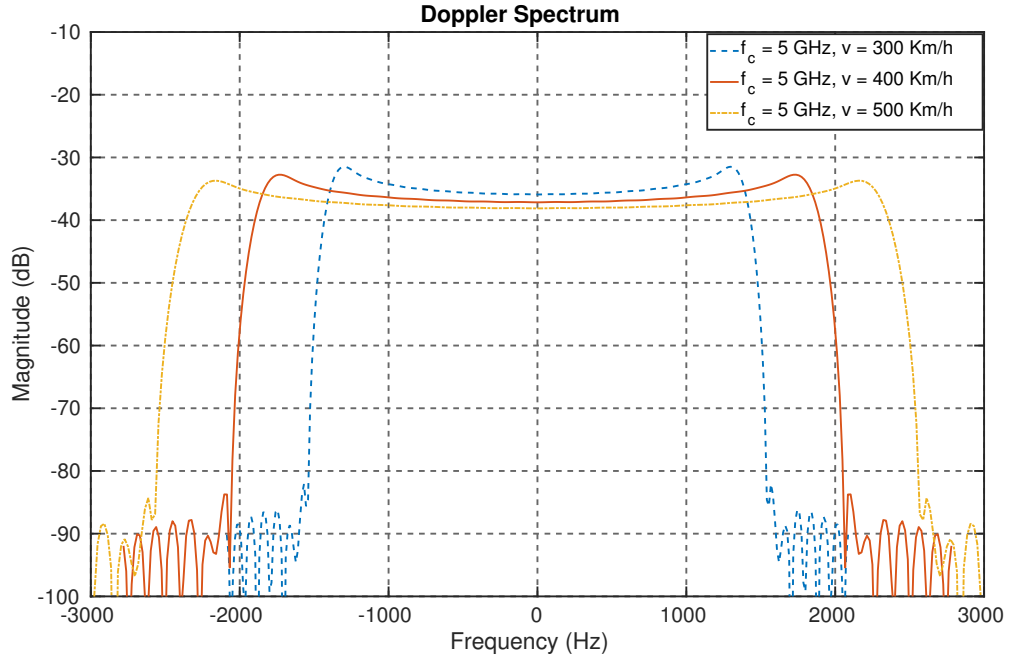


Figure 4.3: Doppler spectrum for LTE-R at different train velocities  $v$  (km/h) = 300, 400 and 500 and  $f_c = 5$  GHz.

our proposed channel model which consists of Doppler shift profile for high speed train and dynamic K-factor for tunnel environment.

#### 4.4 Proposed Channel Model

The tunnel measurement campaign conducted in [20] shows that the amplitude variation inside tunnel follows Rician distribution. In the thesis, we apply the approach used in [69] for single elevation angle  $\theta$  and expand it to a time-varying case. In this thesis, we model  $\theta$  as a function of time and derive time-series  $K$ -factor for the tunnel environment. Figure ?? describes our proposed channel model which is implemented using dynamic K-factor and Doppler shift profile derived using Eq.(4.4). In the following section we discuss the classical two-ray propagation model and mathematical derivation of dynamic K-factor for our proposed channel model.

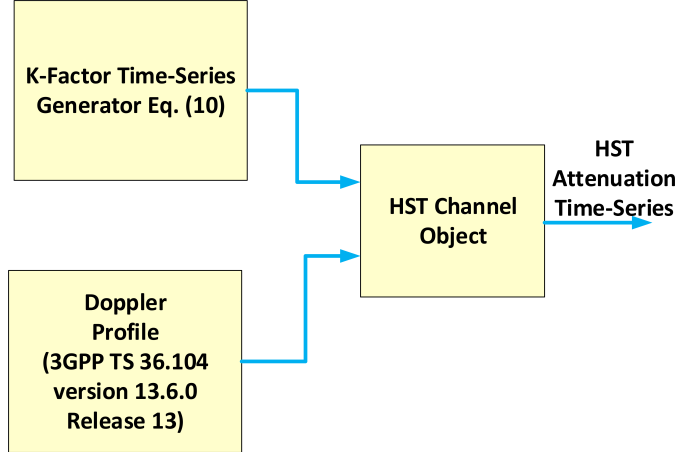


Figure 4.4: HST channel model consisting of time-series K-factor and Doppler shift caused due to velocity of the train.

The reflection coefficient  $\Gamma$  [70] as a function of time  $t$  is given by:

$$\Gamma(t) = \frac{C \sin \theta(t) - \sqrt{(\varepsilon_r - j\chi(t)) - (\cos \theta(t))^2}}{C \sin \theta(t) + \sqrt{(\varepsilon_r - j\chi(t)) - (\cos \theta(t))^2}}, \quad (4.6)$$

where  $C = 1$  is for horizontal polarization, and  $C = \varepsilon_r - j\chi(t)$  for vertical polarization. Furthermore,  $\chi(t)$  is given by:

$$\chi(t) = \frac{\sigma}{\omega(t)\varepsilon_0} = \frac{\sigma}{2\pi f_r(t)\varepsilon_0} = \frac{1.8 \times 10^{10}\sigma}{f_r(t)}. \quad (4.7)$$

with  $\varepsilon_0 = 8.854 \times 10^{-12}$  F/m, and  $\sigma$  is conductivity of the tunnel. The frequency  $f_r(t)$  is the resultant frequency caused by the Doppler shift and is given by:

$$f_r(t) = f_c(t) - f_s(t) \quad (4.8)$$

where  $f_c(t)$  is the sub-carrier frequency, and  $f_s(t)$  is the Doppler shift given by Eq. (4.4).

The phase difference function of  $t$ ,  $\Delta\phi(t)$  between the two reflected paths is given by [24]:

$$\Delta\phi(t) = \frac{2\pi}{\lambda(t)} \left( \sqrt{D_{\text{LOS}}^2 + (h_t + h_r)^2} - \sqrt{D_{\text{LOS}}^2 + (h_t - h_r)^2} \right), \quad (4.9)$$

where  $\lambda(t)$  is the resultant time-varying wavelength at the receiver,  $D_{\text{LOS}}$  is the distance between the transmitter and receiver antennas which is changing dynamically with  $t$ , and both  $h_t$  and  $h_r$  are the heights of the transmitter and receiver antennas, respectively.

The resultant received power  $p_r(t)$  is given by the sum of the LOS received power plus the received multipath power, resulting in:

$$p_r(t) = p_t(t) \left( \frac{\lambda}{4\pi d} \right)^2 G_t G_r \left[ 1 + |\Gamma(t)|^2 + 2|\Gamma(t)| \cos(\angle\Gamma(t) - \angle\Delta\phi(t)) \right] \quad (4.10)$$

which is a function of the transmitter power  $p_t(t)$  and the reflection coefficient  $\Gamma(t)$ , where  $G_t$  and  $G_r$  are the transmitter and receiver antenna gains, respectively. The  $K$ -factor is defined as the ratio of the direct path power and the power in the scattered paths, and is given as:

$$K(t) = \frac{1}{|\Gamma(t)|^2 + 2|\Gamma(t)| \cos(\angle\Gamma(t) - \Gamma(t)\Delta\Phi(t))} \quad (4.11)$$

## 4.5 Summary

This chapter outlined and examined the topics of jamming and anti-jamming techniques, and provided a foundation in communication system theory and advanced equalizer design. Secondly it setup an understanding of Software-Defined Radio, the power of such an architecture, and examples of implementations and existing software for future designs. Next, this thesis will consider a new anti-jamming technique and design an implementation of such a system. After the implementation is investigated, the result of specific experiments on such an implementation will be analyzed.

## Chapter 5

# Implementation

### 5.1 Overview

This chapter outlines the implementation of heterogeneous test-bed for cooperative spectrum sensing using software-defined radios N210, and RTL-SDR and we also describe the simulation test-bed for performance analysis of LTE-R communication system in a tunnel environment. We start with heterogeneous cooperative spectrum sensing where we first describe the experimental setup which is implemented using soft and hard fusion schemes. The sensor nodes which consists of three RTL-SDRs and one USRP N210 are placed in a controlled indoor laboratory environment around 8-10 meters apart. The signal source is being simulated by another USRP N210 which is transmitting a DQPSK signal at 450 MHz. The post-processing is done on a Fusion Center which makes the decision based on global test statistic using both soft and hard decision schemes. The performance of both the schemes are evaluated in a real fading scenario on a hardware test-bed.

We then discuss our LTE-R test-bed implementation in MATLAB and compare the performance for QPSK, 16QAM and 64QAM modulation schemes in a tunnel environment. First we show the results of K-factor variation in a tunnel environment for a high speed train in a tunnel. Using the K-factor we then implement our channel model which also takes into effect the high Doppler shift due to mobility of the train. The bit-error rate curves are generated for the LTE-R modulation schemes for the proposed channel model for high

speed train in a tunnel. Finally, we show a time-varying BER curve for high speed train moving with the velocity  $v$  at discrete timesteps.

## 5.2 Experimental Setup for Heterogeneous CSS

The measurements are performed using software-defined radios (SDRs) and the post processing is conducted on desktop computers. The desktop computer consists of i7 Intel processor with eight cores and 3.41 GHz clock cycle running Ubuntu 16.04. The sensor node network is implemented using RTL-SDR dongles and Ettus Research USRP N210 on GNU Radio Software platform. The measurements are analyzed in MATLAB and measurement plots are generated. Figure 5.1 consists of three RTL-SDRs and two USRP N210s. One USRP N210 in the middle acts as a primary user and other SDRs are sensor nodes. All the SDRs were placed in the lab atleast 5-6 meters away from the primary user.

These sensor nodes collect the spectral data, normalize it and then transmit it to the FC for the detection. For soft data fusion, the data is quantized in the local sensor nodes before it is transmitted to FC due to the limited bandwidth of the overhead channel. The delays caused by different sensor nodes is ignored, as it would require extra computational complexity and it is out of the scope of this thesis. The USRP N210 transmits a DQPSK modulated signal with 4 samples per symbol with the alpha factor of the root raised cosine filter set to 0.35. The transmitter gain and amplitude are varied to get different SNR values for each node. The sensor nodes collect the data for the equivalent of 300,000 energy samples, and each measurement is conducted three times to eliminate any irregularities. The noise variance  $\sigma_n^2$  for each SU is estimated by running each sensor node without any transmission at 450 MHz. The flow-graph is executed multiple times to get a better estimate of noise variance. Once the data is received from all the sensor nodes, Probability of detection is calculated for different received SNR values for all the sensor nodes. To properly evaluate the performance of each of the cooperative spectrum sensing techniques, the average  $P_d$  is calculated for each scheme.

All four sensor nodes have different sampling rates to truly model the heterogeneous environment. The USRP N210 which is also used as a 4<sup>th</sup> sensor node has a very low noise

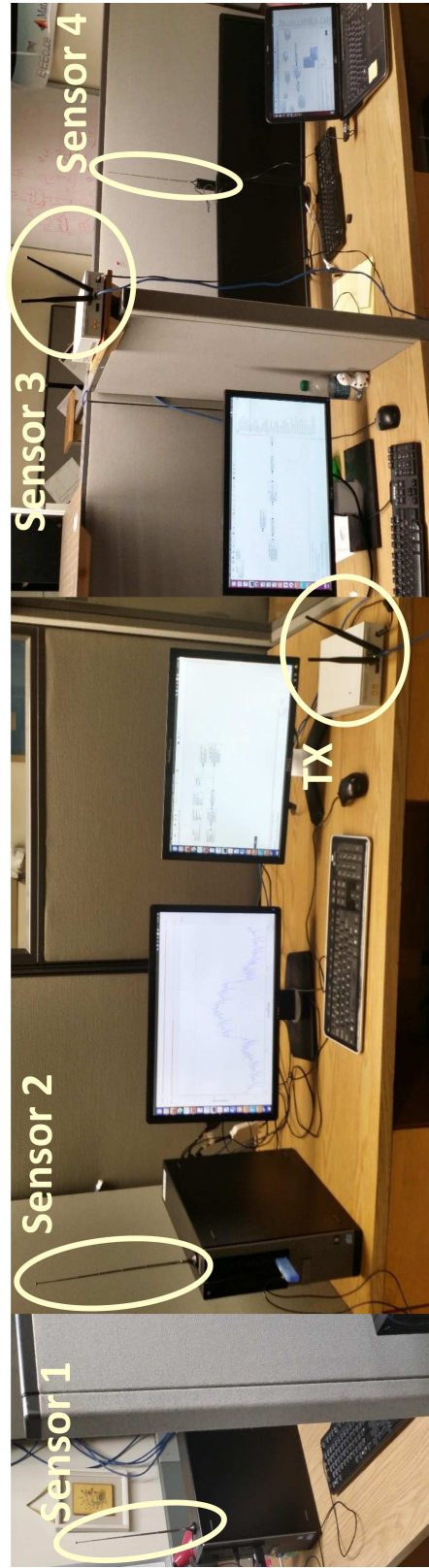


Figure 5.1: Experimental Test-Bed For Cooperative Sensing in Heterogeneous Network. Sensors 1, 2 and 4 are RTL-SDR units, sensor 3 is USRP N210 and TX is another USRP N210 unit which is used as a signal source for this work.

floor compared to the three other and hence can detect a signal with very low SNR. This is a challenging factor for data fusion when the nodes have different operating parameters and FC has to make optimal decisions by combining this varying data. And due to their spatial diversity the node closest to the transmitter will have different SNR compared to the other nodes. All these factors impact the data combining at FC. The GNURadio flow-graph for the sensor nodes is shown in the Figure 5.3. The same flow-graph is used for all sensor nodes with different operating parameters. For USRP N210 node, we replaced the RTL-SDR source with UHD:USRP Source gnuradio block. The central frequency is kept at 450 MHz and the operating parameters of each sensor node is provided in the table. The values of the transmitter amplitude and gain are varied to get the different sets of SNR values which are used for computing  $P_d$  values for each node. The plots are generated in MATLAB by using the data files from gnuradio platform.

### 5.2.1 Sensor Node and Signal Source Setup

To evaluate the performance of the cooperative spectrum sensing, the USRP N210 is used as a transmitter where its gain and amplitude are varied. Figure 5.2 shows the flowgraph used for the transmitter. The flowgraph starts with the random source block which generates the random data between 0 and three, and pass it to the differential phase shift keying (DPSK) modulator block. The DPSK block modulates the signal with differential quadrature phase shift keying (DQPSK) scheme, apply root raise cosine filter with excess bandwidth value of 0.35 and pass it to multiply const block. It is used to control the SNR value and finally the data is dumped into USRP N210 sink which transmits the data over the air where other sensor nodes can estimate the signal presence using soft and hard decision schemes.

The sensor nodes are placed inside the laboratory and are connected to distributed system. Figure 5.3 shows the flowgraph running on the receiver, for flowgraph running on USRP we use UHD:USRP source instead of RTL-SDR source. The frequency around 450 MHz is swepted in regular intervals and the continuous data stream is passed to FFT block which does the forward FFT operation with blackmann harris window. The data is first converted into parallel stream of the FFT size using stream to vector gnu radio

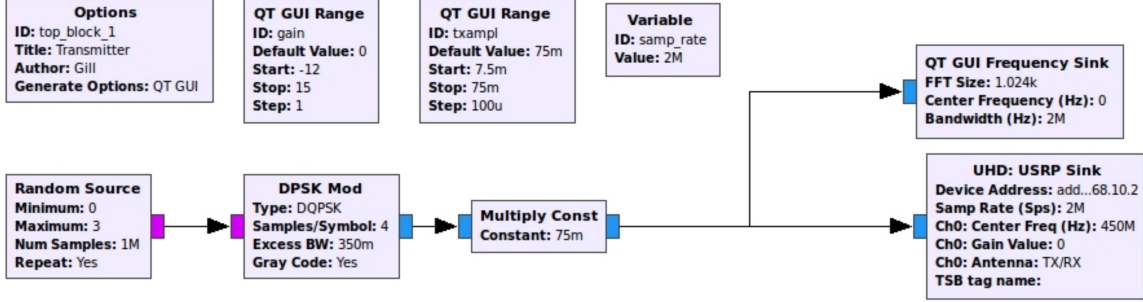


Figure 5.2: GNU Radio Flowgraph For Transmitter Running on USRP N210.

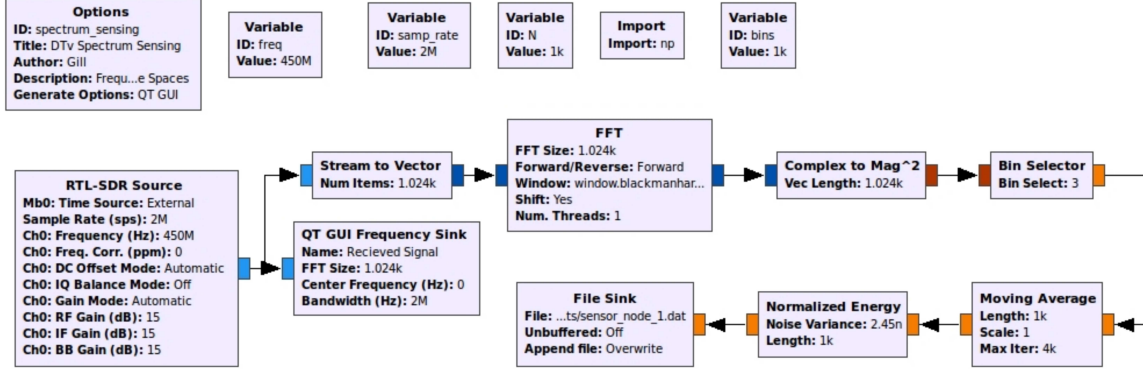


Figure 5.3: GNURadio Flowgraph For USRP and RTL-SDR sensor nodes.

Table 5.1: Operating Characteristics of Sensor Nodes

Nodes	$F_s$	Gain	FFT Size	Bin Size
RTL-SDR-1	1.1 Msps	10 dB	512	2.148 KHz
RTL-SDR-2	1.8 Msps	10 dB	512	3.515 KHz
RTL-SDR-3	2.4 Msps	10 dB	512	4.687 KHz
USRP N210	7.2 Msps	10 dB	512	14.062 KHz

block. We complex to magnitude block converts the complex values into float and take their magnitude. The bin selector block is used to select the bin where the narrow-band signal is being transmitted by the transmitter. We then take the moving average of the values, normalize them and then store it to the file sink. The normalized energy values are collected for each sensor at different SNR values and then post processing is performed in

MATLAB. The operating parameters of each sensor node is provided in the table 5.1.

### 5.3 Hard-Data Fusion Scheme

Cooperative spectrum sensing using hard-data fusion is a proven method for improving the detection performance. In this scheme, all sensor nodes sense the signal source individually and send their sensing decision in the form of 1-bit binary data. For hard data fusion, the noise  $w_q$  can be neglected since the sensor nodes can just transmit their decision statistic in an efficient way, where the floating values are not required. For example, the SUs can just transmit "1" and "0" depending on whether the primary user is present or absent. Furthermore, in the Fusion Center the decision can be made by using the OR, AND, or majority rule algorithms. For the AND decision rule, the FC performs the logical AND operation for all the local decisions and conducts the detection. Similarly, for the OR rule, the logical OR operation is used to decide whether the signal is present or not. Finally, the majority rule conducts majority vote and decides based on it [71, 72]. The  $P_d$  for AND, OR and Majority Rule for R=4 sensor nodes is given by [73]:

$$\begin{aligned} P_{d,AND} &= (P_d)^4 \\ P_{d,MJR} &= 6P_{davg}^2(1 - P_{davg})^2 + 4P_{davg}^3(1 - P_{davg}) + P_{davg}^4 \end{aligned} \quad (5.1)$$

where  $P_{davg}$  is the average probability of detection of the sensor units. Similarly, we can calculate the  $P_{fa}$  for all three schemes by replacing  $P_{davg}$  by  $P_{faavg}$  in Eq (5.4).

### 5.4 Soft-Data Fusion Scheme

In soft-data fusion based cooperative spectrum sensing, information from different CR users is combined to make a decision on the presence or absence of the primary user. In 5.3 we discuss the conventional hard combination where each CR user feedbacks one-bit message regarding whether observed energy is above a certain threshold . In this section, we discuss soft combination of the local test statistic of each sensor nodes and how it is combined to make the decision in the FC. Since in the soft combination accurate energy values from different CR users are utilized to make a decision, this scheme is more accurate and complex

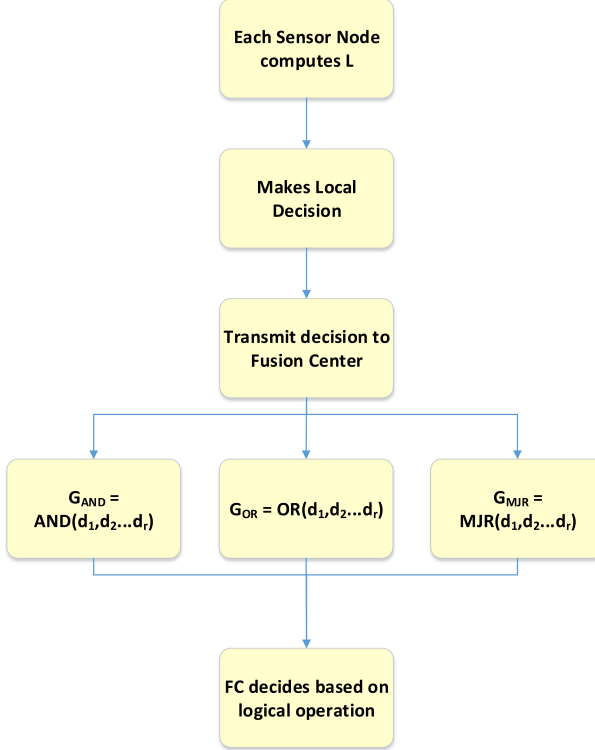


Figure 5.4: Flowchart showing AND, OR and Majority Rule Fusion schemes.

to implement. In this thesis, we discuss two popular soft decision fusion schemes: Maximum Normalized Energy (MNE) scheme and Equal Gain Combining (EGC) scheme.

#### 5.4.1 Maximum Normalized Energy Scheme

The local test statistic in each sensor node is computed and then transmitted to FC after quantization. In this thesis, we are using four sensor nodes equipped with different sensing abilities such as the sampling rates and noise floor. Therefore, the global test statistic  $G$  can be modeled by:

$$G_{MNE} = \max\{\beta_r\}, \quad (5.2)$$

The  $P_{fa}$  and  $P_d$  values for the MNE-CS is given by: [?],

$$P_{fa} = 1 - \prod_{r=1}^R \left( 1 - Q\left(\frac{\tau - 1}{\sqrt{\frac{1}{M_r}} + \sigma_{q,r}}\right) \right), \quad (5.3)$$

$$P_d = 1 - \prod_{r=1}^R \left( 1 - Q\left( \frac{\tau - 1 - \gamma_r}{\sqrt{\frac{1+2\gamma_r}{M_r} + \sigma_{q,r}}} \right) \right). \quad (5.4)$$

where  $\tau$  is the global threshold for MNE,  $M_r$  is the number of samples for  $r^{th}$  sensor node, and  $\sigma_{q,r}$  is the noise variance for the received local test statistic. The algorithm for MNE-CS is illustrated by the flowchart in Figure 5.5.

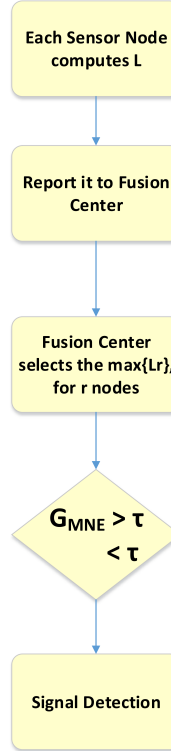


Figure 5.5: Flowchart describing Maximum Normalized Energy Scheme in detail.

#### 5.4.2 Equal Gain Combining Scheme

For EGC, the global decision statistic is the mean of the  $\beta$  values for all the sensor nodes. It has been shown in [19] that the EGC scheme performs better than the MNE scheme in a noisy channel. The EGC scheme can be modeled by:

$$G_{EGC} = \frac{1}{M} \sum_{r=1}^M \beta_r, \quad (5.5)$$

where  $G_{EGC}$  is global test statistic of EGC scheme. The  $P_{fa}$  and  $P_d$  values for the EGC-CS scheme are given by:

$$P_{fa} = Q\left(\frac{\tau - 1}{\sqrt{\frac{1}{R^2} \sum_{r=1}^R \left(\frac{1}{M_r} + \sigma_{q,r}^2\right)}}\right), \quad (5.6)$$

$$P_d = Q\left(\frac{\tau - \frac{1}{R} \sum_{r=1}^R (1 + \gamma_r)}{\sqrt{\frac{1}{R^2} \sum_{r=1}^R \left(\frac{1 + 2\gamma_r}{M_r} + \sigma_{q,r}^2\right)}}\right). \quad (5.7)$$

The algorithm for EGC-CS is also illustrated by the flowchart in Figure ??.

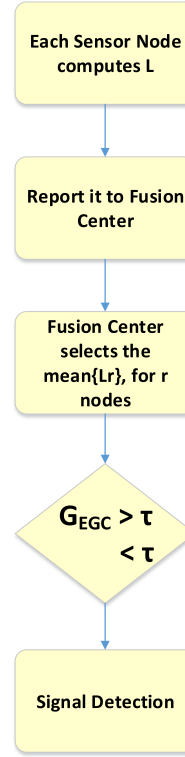


Figure 5.6: Flowchart describing Equal Gain Combining Scheme in detail.

## 5.5 LTE-R Testbed in Matlab

We have implemented the simulation testbed in MATLAB, consisting of a transmitter, a channel and a receiver. The K-factor values for the channel model are obtained from

Table 5.2: Tunnel and Tx/Rx Characteristics

	Dimensions	Simulation Parameters
Tunnel	Width = 8.6 m, Height = 7.3 m	$\varepsilon_r = 5, \sigma = 0.1 \text{ Sm}^{-1}$
Leaky Feeder Cable (Tx)	Height = 6.1 m	$f_c (\text{GHz}) = 2, 3, 5$
Train (Rx)	Height = 4.2 m	$v (\text{km/h}) = 300, 400, 500$

Eq.(??) and are used to generate a time-series BER curve for different modulation schemes used in LTE-R. The values used for the electrical material properties for tunnel walls [74] and its specifications are given in Table 5.2. The relative permittivity for the tunnel walls is taken as  $\varepsilon_r = 5$  and  $\sigma$  is set to 0.1. The simulation is conducted for velocity of  $v(Km/h) = 300, 400$  and  $500 \text{ Km/h}$ . Since the frequency band allocation for LTE-R will most probably be from 2–6 GHz, hence the  $f_c$  values chose are 2, 3 and 5 GHz. The height of the receiver is assumed to be around the length of the train and height of tunnel is chosen as the size of the leaky coaxial cable.

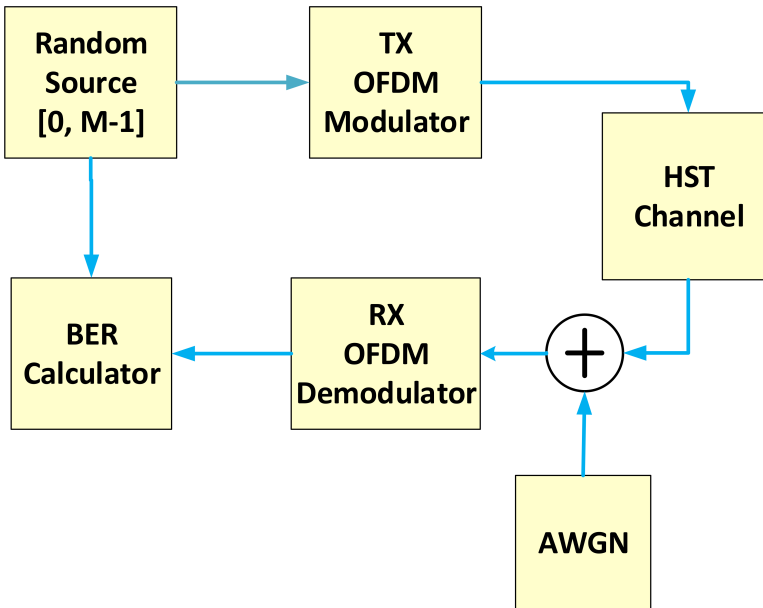


Figure 5.7: Block diagram of a communication system through a HST channel using QPSK, 16-QAM and 64-QAM.

Figure ?? shows the block diagram of the simulation test-bed used for the performance

analysis of LTE-R. The random source block generate the symbol between 0 and M-1, where M = 4,16,64 for QPSK, 16QAM and 64QAM respectively. The data is then modulated with specific modulation type and then pass through the proposed HST channel model. The additive white gaussian noise is added after applying the channel coefficients to the signal data. We then demodulate the data packets and pass it to the ber calculator object which then computes the bit-error rate. The simulations are run for SNR values ranging from 0–20 dB and plots are generated for all three modulation schemes.

## 5.6 Summary

This chapter outlined and examined the topics of jamming and anti-jamming techniques, and provided a foundation in communication system theory and advanced equalizer design. Secondly it setup an understanding of Software-Defined Radio, the power of such an architecture, and examples of implementations and existing software for future designs. Next, this thesis will consider a new anti-jamming technique and design an implementation of such a system. After the implementation is investigated, the result of specific experiments on such an implementation will be analyzed.

## Chapter 6

# Experimental Results

### 6.1 Overview

This chapter outlines the outcomes of the cooperative spectrum sensing using soft and hard decision fusion schemes. The  $P_{davg}$  vs  $SNR$  plot is generated for both the schemes to compare their performance in a real fading scenario on a hardware test-bed. The data files generated using gnuradio are imported in MATLAB for all sensor nodes and the results are derived. As it is expected soft-fusion schemes outperform hard-fusion scheme but as we go to higher SNRs both the schemes generally converges to the same results. For LTE-R performance analysis we have the plot for K-factor variation inside a tunnel for high speed tunnel. We also generated the ber curves for all three modulation schemes proposed for LTE-R and it is evident from the plots for higher K-values we have good connectivity. As the train moves away from the LCXs slot, the K-factor goes down and bit-error rate increases. Finally, we generated the continuous ber curve to test the performance of LTE-R in a discrete timestep manner.

### 6.2 Heterogeneous CSS Results

In this thesis, we implemented the heterogeneous cooperative spectrum sensing (CSS) using both hard and soft data fusion schemes. We start by collecting the data across 450 MHz band for all sensor nodes in a distributed manner. The spectrum sensing data is nor-

malized for both soft and hard data fusion schemes using the same operational parameters to compare their performance accurately. The measurements are performed using software-defined radios (SDRs) and the post processing is conducted on desktop computers. The desktop computer consists of i7 Intel processor with eight cores and 3.41 GHz clock cycle running Ubuntu 16.04. The sensor node network is implemented using RTL-SDR dongles and Ettus Research USRP N210 on GNU Radio Software platform. These sensor nodes collect the spectral data, normalize it and then transmit it to the FC for the detection. For soft data fusion, the data is quantized in the local sensor nodes before it is transmitted to FC due to the limited bandwidth of the overhead channel.

### 6.2.1 Hard Decision Combining

The Figure 6.1 shows the shows the  $P_{davg}$  versus  $SNR_{avg}$  for all four sensor nodes. It can be seen that OR performs the best while AND performs the worst in a fading channel. The SN R avg was computed by taking the mean of all the SNRs for the sensor nodes. The SNR was varied for each sensor node by varying the transmitter amplitude and gain in the gnuradio flowgraph.

In Figure 6.2 the ROC characteristics for the hard decision combining at two different  $SNR_{avg}$  for all three hard data fusion schemes are provided. It is pretty evident from the plot that OR scheme performs better than both AND and majority rule scheme. The AND scheme performs the worst because it depends on all sensor nodes to have same decision which is very difficult in a real fading environment. For lower SNR values OR outperform majority rule by a large margin but as we go to higher SNR values their performance converges.

### 6.2.2 Soft Decision Combining

The Figure 6.3 shows the  $P_{davg}$  vs  $SNR_{avg}$  for both soft and hard data fusion schemes. MNE and OR scheme overlap on the plot because in MNE scheme we take the maximum normalized energy and compare it the global test statistic, whereas in OR scheme we estimate the signal source by either of sensor node decision. This makes both the scheme almost same and this is visible in the results. The EGC scheme performs the best because it takes

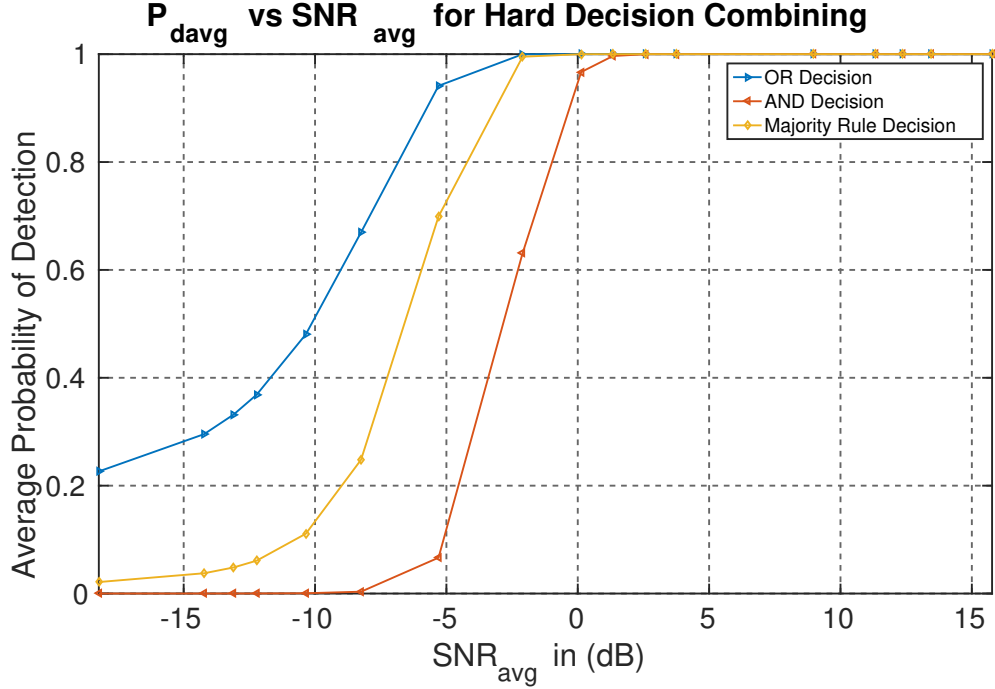


Figure 6.1: Probability of Detection versus  $SNR_{avg}$  For Hard Decision Combining.

into consideration all the sensor nodes and it's global test statistic gives equal weightage to all sensor nodes. AND scheme performs the worst as it was expected. It is very important to understand that at higher SNR values,  $SNR_{avg} \geq 2$  dB, we see all schemes converging to the same decisions. This tells us that in noiseless environment we can choose hard fusion schemes because of their implementation complexity and we can select soft fusion in severe fading environment as they tend to be more accurate in these scenarios.

### 6.3 HST LTE-R in a Tunnel

Using LTE System Toolbox provided by MATLAB we generated Figure ?? which shows the received resource grid without equalization. The frame worth of data was modulated with QPSK, 16QAM and 64QAM for equal number of subcarriers and mapped to symbol in a subframe. We generate ten subframes individually and create one frame after merging all subframes. The frame is passed through our proposed high speed train channel model, with additive white gaussian noise added. We can see that without equalization the received

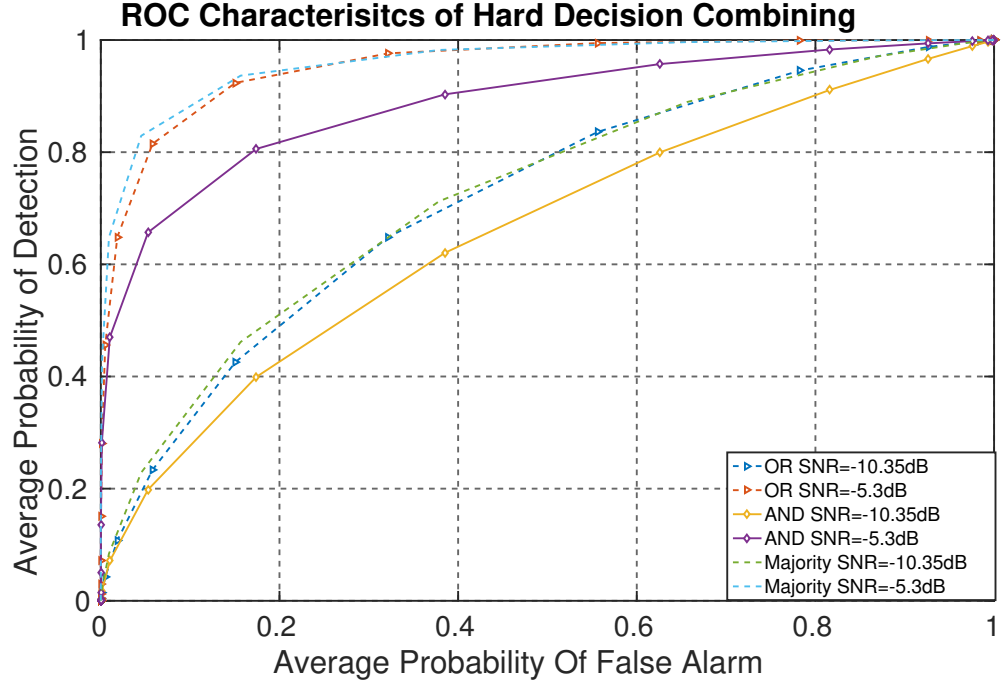


Figure 6.2: ROC Characteristics for Hard Decision Combining with Different SNRs.

resourceed grid has lot of errors and will lead to numerous retransmissions.

### 6.3.1 K-factor in a Tunnel

In Figure ??, we calculated the K-factor for the HST inside a tunnel with velocity  $v = 500$  km/h for different center frequencies. It shows the variation of the Rician K-factor with the distance between the transmitter and receiver as the train is moving along the tunnel. We computed the K-factor for a leaky cable with periodic slots separated by distance  $d$  in fixed time-steps. The plot shows that the K-factor varies significantly over a short distances. Therefore, assuming a single K-factor for the channel model is not accurate, we use time-series K-factor to do our channel modeling.

### 6.3.2 BER Performance

To show the impact of varying K-factor on the channel, we computed the BER curve for different modulation schemes of LTE-R with different K-factors. Fig. 6.6a shows the BER

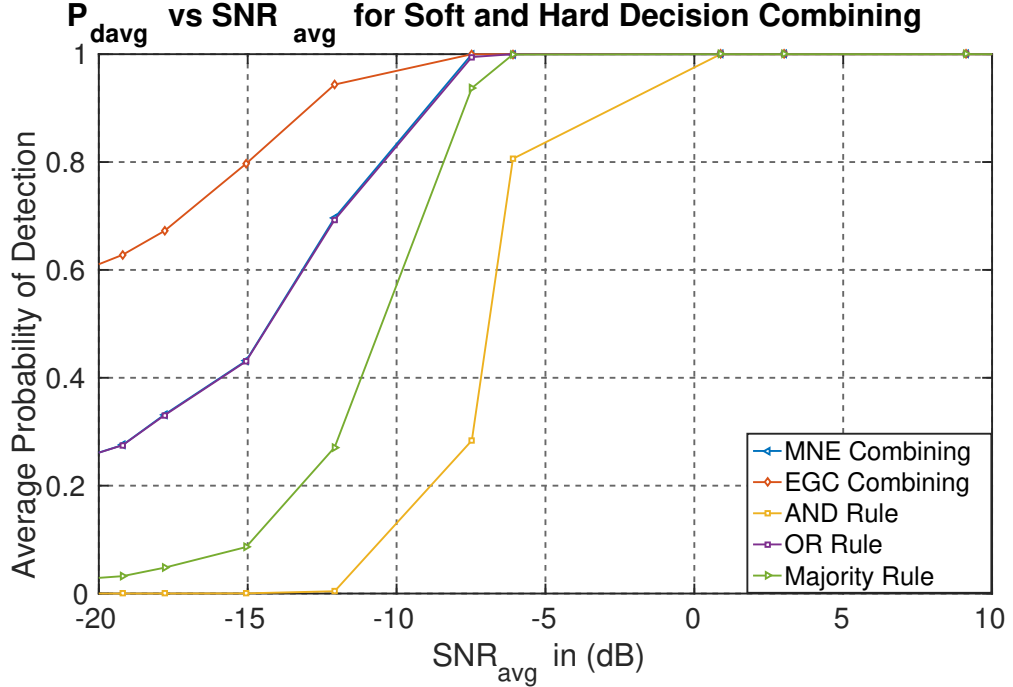


Figure 6.3: Probability of Detection versus  $SNR_{avg}$  For Soft and Hard Decision Combining.

versus SNR performance for QPSK modulation for different K-factors of the tunnel channel model. The figure clearly demonstrates for higher K-factor we have a better performance while performance degrades as K-factor goes low. Fig. 6.6b shows the  $E_b/N_0$  versus BER for 16-QAM and as we can see the BER is higher compared to QPSK. Fig. 6.6c shows the  $E_b/N_0$  versus BER for 64-QAM for different K-factors. And finally we compare all the modulation schemes for the best and worst K-factor in Fig. 6.6d.

In Fig. ?? we calculate the BER performance for a high speed train in discrete time-steps. As the train moves towards the LCX slot the SNR goes high and the SNR decreases as the train moves away. This trend can be seen in the plot, as we move towards the slot the BER curve decreases and it starts increases once we move. It is important to consider here that due to the varying nature of K-factor the BER curve also varies significantly. Hence, by considering the time-varying nature of K-factor we can have a better performance analysis.

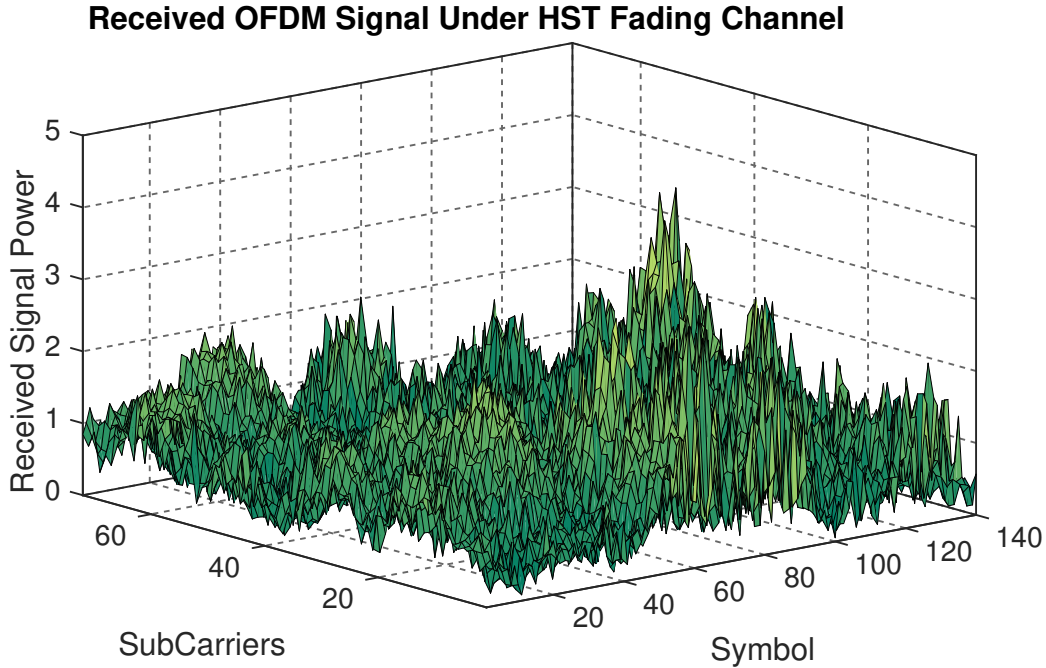


Figure 6.4: Received LTE-R OFDM signal under HST Ricean Fading Environment.

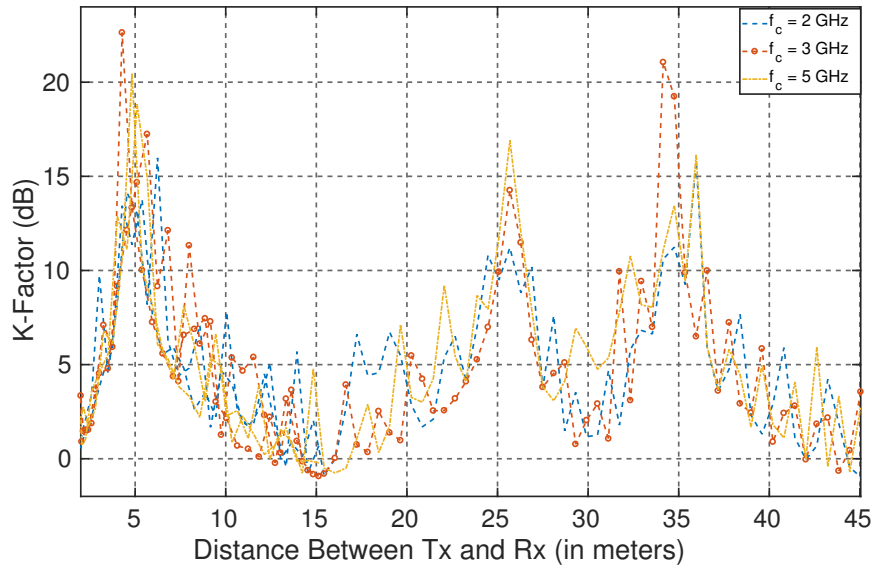


Figure 6.5: K-factor versus  $D_{LOS}$  for different center frequencies  $f_c = 2, 3$  and 5 GHz.

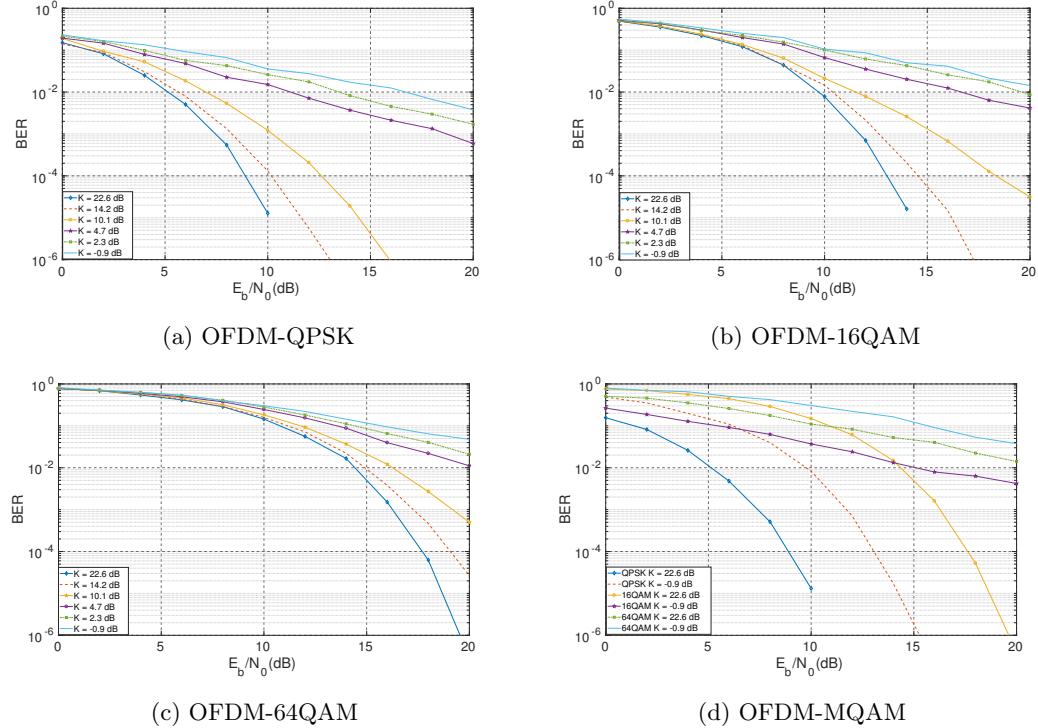


Figure 6.6: Comparison of  $E_b/N_0$  verus BER for LTE-R OFDM modulation with different  $K$ -factors. The first three sub-figures shows the  $E_b/N_0$  versus BER for individual modulation schemes employed in LTE-R and in last plot we compare all the modulation schemes for different  $K$ -factors.

## 6.4 Summary

We analyzed the BER performance of a LTE-R system for high speed trains inside tunnel environments using our proposed channel model. For the implementation of our channel, we first derived the time-series K-factor function using the classical two-ray propagation model. We then analyzed the LTE-R performance under our channel model for different modulation schemes for various K-factors. Finally, we compared all the modulation schemes under worst and best K-factor, and we observed that for low  $E_b/N_0$  sub-carriers must be modulated with QPSK for maintaining reliable communication link.

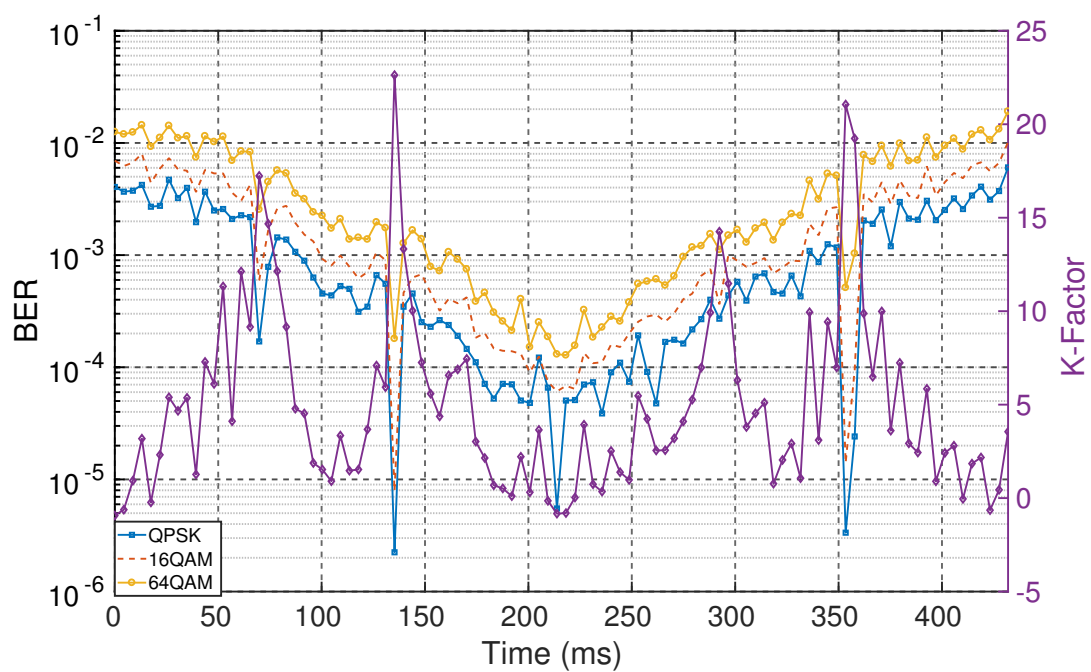


Figure 6.7: BER variation with time for HST with different modulation schemes of LTE-R. As the train moves towards the antenna the general trend of BER goes down with small-scale fluctuations due to varying K-factor.

## Chapter 7

# Conclusions

This chapter summarizes the work as part of this project and then suggests related research that can be performed in the future. The research achievements includes implementation of test-bed for cooperative spectrum sensing in heterogeneous network, the performance measure of both soft and hard data fusion schemes in a real fading scenario. The simulation test-bed is implemented in MATLAB to test the performance of LTE-R in our proposed channel. The proposed channel is built on two-ray propagation model with time-series K-factor which we have derived mathematically and also uses Doppler shift profile for high speed trains. The future work section describes how we can take the mobility effect into the cooperative spectrum sensing and then test the performance of soft and hard fusion schemes in a mobile scenario. For LTE-R for future work we will use LTE antenna toolbox provided by MATLAB to implement the simulation test-bed which is more realistic and close to the actual system.

### 7.1 Research Outcomes

- We analyzed the BER performance of a LTE-R system for high speed trains inside tunnel environments using our proposed channel model. For the implementation of our channel, we first derived the time-series K-factor function using the classical two-ray propagation model.

- We then analyzed the LTE-R performance under our channel model for different modulation schemes for various K-factors. Finally, we compared all the modulation schemes under worst and best K-factor, and we observed that for low  $E_b/N_0$  sub-carriers must be modulated with QPSK for maintaining reliable communication link.
- The last plot shows the BER curve for discrete time-step when the train is moving with a velocity of 500 Km/h and carrier frequency for all modulation scheme is set to 3 GHz. The plot is also overlayed with continuous K-factor variation with the propagation of the train. It can be observed from the plot that as the K-factor goes high the BER drops, which represents the train moving towards the LCX slot.
- As the train move away from the slot the BER starts increasing. For reliable and efficient communication links the sub-carriers have to be modulated with QPSK for low K-factor values, or more LTE repeaters are required inside the tunnel to get good connectivity. However, the most important factor that has to be taken into consideration is the real-time channel equalization to reduce the BER rate.

## 7.2 Future Work

- In this paper, we conducted an experimental study for cooperative spectrum sensing using normalized energy detection for both soft and hard decision combining techniques. It was found that the soft fusion schemes works better than hard decision for real fading environment with low SNR values.
- For higher values, all schemes converged to the same decision which led us to conclude that hard fusion schemes pays better when the environment is less noisy due to their low complexity as compared to soft fusion. For future work, it is worth exploring an increase in the number of nodes and adding mobility for the testing the performance of heterogeneous networks in a time-variant channel.

# Bibliography

- [1] I. F. Akyildiz, W.-Y. Lee, M. C. Vuran, and S. Mohanty, “Next generation/dynamic spectrum access/cognitive radio wireless networks: A survey,” *Computer networks*, vol. 50, no. 13, pp. 2127–2159, 2006.
- [2] Q. Zhao and B. M. Sadler, “A survey of dynamic spectrum access,” *IEEE signal processing magazine*, vol. 24, no. 3, pp. 79–89, 2007.
- [3] A. M. Wyglinski and D. Pu, *Digital communication systems engineering with software-defined radio*. Artech House, 2013.
- [4] H. Urkowitz, “Energy detection of unknown deterministic signals,” *Proceedings of the IEEE*, vol. 55, no. 4, pp. 523–531, 1967.
- [5] D. Cabric, S. M. Mishra, and R. W. Brodersen, “Implementation issues in spectrum sensing for cognitive radios,” in *Signals, systems and computers, 2004. Conference record of the thirty-eighth Asilomar conference on*, vol. 1. Ieee, 2004, pp. 772–776.
- [6] R. Tandra and A. Sahai, “Fundamental limits on detection in low snr under noise uncertainty,” in *Wireless Networks, Communications and Mobile Computing, 2005 International Conference on*, vol. 1. IEEE, 2005, pp. 464–469.
- [7] S. M. Mishra, A. Sahai, and R. W. Brodersen, “Cooperative sensing among cognitive radios,” in *Communications, 2006. ICC’06. IEEE International conference on*, vol. 4. IEEE, 2006, pp. 1658–1663.
- [8] A. Ghasemi and E. S. Sousa, “Impact of user collaboration on the performance of

- sensing-based opportunistic spectrum access,” in *Vehicular Technology Conference, 2006. VTC-2006 Fall. 2006 IEEE 64th.* IEEE, 2006, pp. 1–6.
- [9] U. G.-R. F. Group, “Gsm-r functional requirement specification (FRS),” UIC, Paris, France UIC EIRENE Technology Report, Tech. Rep. UIC Code 950, Version 7.3.0, 2012.
  - [10] G. T. 36.201, “Evolved universal terrestrial radio access (E-UTRA); lte physical layer; general description,” 3GPP, Sophia Antipolis, France, Tech. Rep. version 12.2.0, Release 12, 2015.
  - [11] K. Masur and D. Mandoc, “Lte/saethe future railway mobile radio system? long term visions on railway mobile radio technologies,” *International Union of Railways (UIC), Technical Report*, vol. 1, 2009.
  - [12] G. Tingting and S. Bin, “A high-speed railway mobile communication system based on lte,” in *Electronics and Information Engineering (ICEIE), 2010 International Conference On.* IEEE, 2010, pp. V1–414.
  - [13] K. Guan, Z. Zhong, and B. Ai, “Assessment of lte-r using high speed railway channel model,” in *Communications and Mobile Computing (CMC), 2011 Third International Conference on.* IEEE, 2011, pp. 461–464.
  - [14] H. Wei, Z. Zhong, K. Guan, and B. Ai, “Path loss models in viaduct and plain scenarios of the high-speed railway,” in *Communications and Networking in China (CHINACOM), 2010 5th International ICST Conference on.* IEEE, 2010, pp. 1–5.
  - [15] D. G. Dudley, M. Lienard, S. F. Mahmoud, and P. Degauque, “Wireless propagation in tunnels,” *IEEE Antennas and Propagation Magazine*, vol. 49, no. 2, pp. 11–26, 2007.
  - [16] J. Ma, G. Zhao, and Y. Li, “Soft combination and detection for cooperative spectrum sensing in cognitive radio networks,” *IEEE Transactions on Wireless Communications*, vol. 7, no. 11, pp. 4502–4507, 2008.

- [17] B. Shen, T. Cui, K. Kwak, C. Zhao, and Z. Zhou, "An optimal soft fusion scheme for cooperative spectrum sensing in cognitive radio network," in *Wireless Communications and Networking Conference, 2009. WCNC 2009. IEEE*. IEEE, 2009, pp. 1–5.
- [18] H. Rifà-Pous, M. J. Blasco, and C. Garrigues, "Review of robust cooperative spectrum sensing techniques for cognitive radio networks," *Wireless Personal Communications*, vol. 67, no. 2, pp. 175–198, 2012.
- [19] Y. Zeng, Y.-C. Liang, S. Zheng, and E. C. Peh, "Optimal cooperative sensing and its robustness to decoding errors," in *Communications (ICC), 2011 IEEE International Conference on*. IEEE, 2011, pp. 1–5.
- [20] J.-M. Molina-Garcia-Pardo, M. Lienard, A. Nasr, and P. Degauque, "Wideband analysis of large scale and small scale fading in tunnels," in *ITS Telecommunications, 2008. ITST 2008. 8th International Conference on*. IEEE, 2008, pp. 270–273.
- [21] T. Liu, X. Ma, R. Zhao, H. Dong, and L. Jia, "Doppler shift estimation for high-speed railway scenario," in *2016 IEEE 83rd Vehicular Technology Conference (VTC Spring)*, May 2016, pp. 1–5.
- [22] Usrp. [Online]. Available: <https://www.ettus.com/product/category/USRP-Embedded-Series/>
- [23] Rtl-sdr. [Online]. Available: <http://www rtl-sdr com/>
- [24] T. S. Rappaport *et al.*, *Wireless communications: principles and practice*. prentice hall PTR New Jersey, 1996, vol. 2.
- [25] A. Hashimoto, H. Yoshino, and H. Atarashi, "Roadmap of imt-advanced development," *IEEE Microwave Magazine*, vol. 9, no. 4, pp. 80–88, Aug 2008.
- [26] V. Chandrasekhar, J. G. Andrews, and A. Gatherer, "Femtocell networks: a survey," *IEEE Communications Magazine*, vol. 46, no. 9, pp. 59–67, September 2008.
- [27] F. Boccardi, R. Heath, A. Lozano, T. L. Marzetta, and P. Popovski, "Five disruptive technology directions for 5G," *IEEE Communications Magazine*, vol. 52, no. 2, pp. 74–80, 2014.

- [28] C.-X. Wang, F. Haider, X. Gao, X.-H. You, Y. Yang, D. Yuan, H. Aggoun, H. Haas, S. Fletcher, and E. Hepsaydir, “Cellular architecture and key technologies for 5G wireless communication networks,” *IEEE Communications Magazine*, vol. 52, no. 2, pp. 122–130, 2014. [Online]. Available: <http://ieeexplore.ieee.org/lpdocs/epic03/wrapper.htm?arnumber=6736752>
- [29] T. S. Rappaport, S. Sun, R. Mayzus, H. Zhao, Y. Azar, K. Wang, G. N. Wong, J. K. Schulz, M. Samimi, and F. Gutierrez, “Millimeter wave mobile communications for 5g cellular: It will work!” *IEEE Access*, vol. 1, pp. 335–349, 2013.
- [30] H. Elgala, R. Mesleh, H. Haas, and B. Pricope, “Ofdm visible light wireless communication based on white leds,” in *2007 IEEE 65th Vehicular Technology Conference - VTC2007-Spring*, April 2007, pp. 2185–2189.
- [31] S. Y. Seidel and H. W. Arnold, “Propagation measurements at 28 ghz to investigate the performance of local multipoint distribution service (lmds),” in *Global Telecommunications Conference, 1995. GLOBECOM '95., IEEE*, vol. 1, Nov 1995, pp. 754–757 vol.1.
- [32] M. Nekovee, “Dynamic spectrum access with cognitive radios: Future architectures and research challenges,” in *2006 1st International Conference on Cognitive Radio Oriented Wireless Networks and Communications*, June 2006, pp. 1–5.
- [33] J. Mitola, “Cognitive radio for flexible mobile multimedia communications,” in *Mobile Multimedia Communications, 1999. (MoMuC '99) 1999 IEEE International Workshop on*, 1999, pp. 3–10.
- [34] Mimo. [Online]. Available: <https://massivemimo.eu/>
- [35] A. Laya, L. Alonso, and J. Alonso-Zarate, “Is the random access channel of lte and lte-a suitable for m2m communications? a survey of alternatives.” *IEEE Communications Surveys and Tutorials*, vol. 16, no. 1, pp. 4–16, 2014.
- [36] M. Chen, J. Wan, S. González-Valenzuela, X. Liao, and V. C. Leung, “A survey of

- recent developments in home m2m networks.” *IEEE Communications Surveys and Tutorials*, vol. 16, no. 1, pp. 98–114, 2014.
- [37] F. Rusek, D. Persson, B. K. Lau, E. G. Larsson, T. L. Marzetta, O. Edfors, and F. Tufvesson, “Scaling up mimo: Opportunities and challenges with very large arrays,” *IEEE Signal Processing Magazine*, vol. 30, no. 1, pp. 40–60, 2013.
  - [38] A. M. Wyglinski, M. Nekovee, and T. Hou, *Cognitive radio communications and networks: principles and practice*. Academic Press, 2009.
  - [39] X. Hong, C.-X. Wang, M. Uysal, X. Ge, and S. Ouyang, “Capacity of hybrid cognitive radio networks with distributed vaas,” *IEEE Transactions on Vehicular Technology*, vol. 59, no. 7, pp. 3510–3523, 2010.
  - [40] W. Roh, J.-Y. Seol, J. Park, B. Lee, J. Lee, Y. Kim, J. Cho, K. Cheun, and F. Aryanfar, “Millimeter-wave beamforming as an enabling technology for 5g cellular communications: Theoretical feasibility and prototype results,” *IEEE communications magazine*, vol. 52, no. 2, pp. 106–113, 2014.
  - [41] H. T. Friis, “A note on a simple transmission formula,” *Proceedings of the IRE*, vol. 34, no. 5, pp. 254–256, 1946.
  - [42] X. Ge, H. Cheng, G. Mao, Y. Yang, and S. Tu, “Vehicular communications for 5g cooperative small-cell networks,” *IEEE Transactions on Vehicular Technology*, vol. 65, no. 10, pp. 7882–7894, 2016.
  - [43] G. Araniti, C. Campolo, M. Condoluci, A. Iera, and A. Molinaro, “Lte for vehicular networking: a survey,” *IEEE Communications Magazine*, vol. 51, no. 5, pp. 148–157, 2013.
  - [44] S. Mumtaz, K. M. S. Huq, and J. Rodriguez, “Direct mobile-to-mobile communication: Paradigm for 5g,” *IEEE Wireless Communications*, vol. 21, no. 5, pp. 14–23, 2014.
  - [45] J. Mitola and G. Q. Maguire, “Cognitive radio: making software radios more personal,” *IEEE Personal Communications*, vol. 6, no. 4, pp. 13–18, Aug 1999.

- [46] B. Barker, A. Agah, and A. M. Wyglinski, "Mission-oriented communications properties for software-defined radio configuration," *Cognitive Radio Networks*, p. 435, 2008.
- [47] S. Haykin, "Cognitive radio: brain-empowered wireless communications," *IEEE journal on selected areas in communications*, vol. 23, no. 2, 2005.
- [48] T. R. Newman, B. A. Barker, A. M. Wyglinski, A. Agah, J. B. Evans, and G. J. Minden, "Cognitive engine implementation for wireless multicarrier transceivers," *Wireless communications and mobile computing*, vol. 7, no. 9, pp. 1129–1142, 2007.
- [49] T. R. Newman, R. Rajbanshi, A. M. Wyglinski, J. B. Evans, and G. J. Minden, "Population adaptation for genetic algorithm-based cognitive radios," *Mobile networks and applications*, vol. 13, no. 5, pp. 442–451, 2008.
- [50] G. Yang, J. Wang, J. Luo, O. Y. Wen, H. Li, Q. Li, and S. Li, "Cooperative spectrum sensing in heterogeneous cognitive radio networks based on normalized energy detection," *IEEE Transactions on vehicular technology*, vol. 65, no. 3, pp. 1452–1463, 2016.
- [51] Y. Zeng and Y.-C. Liang, "Eigenvalue-based spectrum sensing algorithms for cognitive radio," *IEEE transactions on communications*, vol. 57, no. 6, 2009.
- [52] J. Mitola, "Software radios-survey, critical evaluation and future directions," in [*Proceedings/ NTC-92: National Telesystems Conference*, May 1992, pp. 13/15–13/23.
- [53] R. I. Lackey and D. W. Upmal, "Speakeasy: the military software radio," *IEEE Communications Magazine*, vol. 33, no. 5, pp. 56–61, May 1995.
- [54] Xilinx-spartan-3a. [Online]. Available: <https://www.xilinx.com/products/silicon-devices/fpga/xa-spar>
- [55] Gnu radio. [Online]. Available: <http://gnuradio.org/>
- [56] V. Bose, M. Ismert, M. Welborn, and J. Guttag, "Virtual radios," *IEEE Journal on selected areas in communications*, vol. 17, no. 4, pp. 591–602, 1999.

- [57] T. F. Collins, “Implementation and analysis of spectral subtraction and signal separation in deterministic wide-band anti-jamming scenarios,” Ph.D. dissertation, Worcester Polytechnic Institute, 2013.
- [58] Matlab2017a. [Online]. Available: <https://www.mathworks.com/products/matlab.html>
- [59] G. Tingting and S. Bin, “A high-speed railway mobile communication system based on lte,” in *Electronics and Information Engineering (ICEIE), 2010 International Conference On*, vol. 1. IEEE, 2010, pp. V1–414.
- [60] K. N, N. T, and N. T, “Leaky coaxial cable,” May 7 1974, uS Patent 3,810,186. [Online]. Available: <https://www.google.com/patents/US3810186>
- [61] A. Motley and D. Palmer, “Directed radio coverage within buildings,” in *Proc. IEE Conf. Radio spectrum conversion techniques*, 1983.
- [62] A. A. Saleh, A. Rustako, and R. Roman, “Distributed antennas for indoor radio communications,” *IEEE Transactions on Communications*, vol. 35, no. 12, pp. 1245–1251, 1987.
- [63] H. Cao and Y. Zhang, “Radio propagation along a radiated mode leaky coaxial cable in tunnels,” in *Microwave Conference, 1999 Asia Pacific*, vol. 2. IEEE, 1999, pp. 270–272.
- [64] T. Takatsu, “The history and future of high-speed railways in japan,” *Japan Railway & Transport Review*, vol. 48, pp. 6–21, 2007.
- [65] M. Pätzold, *Mobile radio channels*. John Wiley & Sons, 2011.
- [66] H. Wang, F. R. Yu, and H. Jiang, “Modeling of radio channels with leaky coaxial cable for lte-m based cbtc systems,” *IEEE Communications Letters*, vol. 20, no. 5, pp. 1038–1041, 2016.
- [67] F. F. Digham, M.-S. Alouini, and M. K. Simon, “On the energy detection of unknown signals over fading channels,” in *Communications, 2003. ICC’03. IEEE International Conference on*, vol. 5. Ieee, 2003, pp. 3575–3579.

- [68] 3rd Generation Partnership Project, “technical specification group radio access network;spatial channel model for mimo simulations,” 3GPP, Sophia Antipolis, France, Tech. Rep. TR 25.996 V6.1.0, 2003.
- [69] P. V. R. Ferreira and A. M. Wyglinski, “Performance analysis of uhf mobile satellite communication system experiencing ionospheric scintillation and terrestrial multipath fading,” in *Vehicular Technology Conference (VTC Fall), 2015 IEEE 82nd*. IEEE, 2015, pp. 1–5.
- [70] D. Jordane *et al.*, *Electromagnetic waves and radiating systems*. Prentice-Hall Of India Private Limited; New Delhi, 1967.
- [71] A. Ghasemi and E. S. Sousa, “Collaborative spectrum sensing for opportunistic access in fading environments,” in *New Frontiers in Dynamic Spectrum Access Networks, 2005. DySPAN 2005. 2005 First IEEE International Symposium on*. IEEE, 2005, pp. 131–136.
- [72] J. Duan and Y. Li, “Performance analysis of cooperative spectrum sensing in different fading channels,” in *Computer Engineering and Technology (ICCET), 2010 2nd International Conference on*, vol. 3. IEEE, 2010, pp. V3–64.
- [73] S. Nallagonda, S. D. Roy, A. Chandra, and S. Kundu, “Performance of cooperative spectrum sensing in hoyt fading channel under hard decision fusion rules,” in *Computers and Devices for Communication (CODEC), 2012 5th International Conference on*. IEEE, 2012, pp. 1–4.
- [74] K. Arshad, F. Katsriku, A. Lasebae *et al.*, “Effects of different parameters on attenuation rates in circular and arch tunnels,” *PIERS Online*, vol. 3, no. 5, pp. 607–611, 2007.

## Appendix A

# Appendix: Heterogeneous Cooperative Spectrum Sensing Code

### A.1 harddecisionpdroc.m

```
% Hard-Decision Combining Results For Sensor Nodes
clc;
close all;
clear all;

%% Parameter Initialization
N = 32;
k=4;%sensor nodes..
variance = 24.32e-9;
pfa = 0.05;
threshold = (qfuncinv(pfa)+sqrt(N)).*sqrt(N)*2*variance;
snrthreotical = -18:0.5:20;
snrlinear = 10.^ (snrthreotical/10);

%% SNR values from USRP and RTL-SDR
snrpracticalavg = [-18.23,-14.22,-13.1,-12.22,-10.35,-8.25,-5.3,-2.1,0.13,...]
```

```

1.34,2.58,3.76,8.98,11.33,12.35,13.45,15.77];
snrlinearprac = 10.^ (snrpracticalavg/10);
%% Computing Detection Probability and ROC Characteristics
pdprac = qfunc((threshold-2*N*variance.* (1+snrlinearprac))./...
    (sqrt(N.* (1+2*snrlinearprac)) * (2*variance)));
pdpracor = 1-(1-pdprac).^4;
pdpracand = pdprac.^4;
tmp1 = (1-pdprac).^2;
tmp2 = (1-pdprac);
pdpracmjr = (6*pdprac.^2).*tmp1+(4*pdprac.^3).*tmp2+pdprac.^4;

pfapracor = 1-(1-pfa).^4;
pfapracand = pfa.^4;
tmp1 = (1-pfa).^2;
tmp2 = (1-pfa);
pfapracmjr = (6*pfa.^2).*tmp1+(4*pfa.^3).*tmp2+pfa.^4;

%% ROC Characteristics...
figure(1)
hold on;
grid on;
plot(pfapracor,pdpracor(:,5), '-->', 'LineWidth', 2, 'MarkerFaceColor', 'auto');
plot(pfapracor,pdpracor(:,7), '-->', 'LineWidth', 2, 'MarkerFaceColor', 'auto');
plot(pfapracand,pdpracand(:,5), '-d', 'LineWidth', 2, 'MarkerFaceColor', 'auto');
plot(pfapracand,pdpracand(:,7), '-d', 'LineWidth', 2, 'MarkerFaceColor', 'auto');
plot(pfapracmjr,pdpracmjr(:,5), '--', 'LineWidth', 2, 'MarkerFaceColor', 'auto');
plot(pfapracmjr,pdpracmjr(:,7), '--', 'LineWidth', 2, 'MarkerFaceColor', 'auto');
xlabel('Average Probability Of False Alarm');
ylabel('Average Probability of Detection');
title('ROC Characterisitcs of Hard Decision Combining');
hold off;
set(gca, 'fontsize', 30, 'box', 'on', 'LineWidth', 2, 'GridLineStyle', '--', 'GridAlpha'
    , 0.7);
lgd = legend('OR SNR=-10.35dB', 'OR SNR=-5.3dB', 'AND SNR=-10.35dB', ...
    'AND SNR=-5.3dB', 'Majority SNR=-10.35dB', 'Majority SNR=-5.3dB');
lgd.FontSize=20;

```

```

%% Probability of detection
figure(2)
hold on;
grid on;
plot(snrpracticalavg,pdpracor,'->','LineWidth',2);
plot(snrpracticalavg,pdpracand,'-<','LineWidth',2);
plot(snrpracticalavg,pdpracmjr,'-d','LineWidth',2);
xlabel('SNR-{avg} in (dB)');
ylabel('Average Probability of Detection');
title('P_{avg} vs SNR_{avg} for Hard Decision Combining');
hold off;
set(gca,'fontsize',30,'box','on','LineWidth',2,'GridLineStyle','--','GridAlpha'
,0.7);
lgd = legend('OR Decision','AND Decision','Majority Rule Decision');
lgd.FontSize=20;
axis([-18.23 15.77 0 1])

```

## A.2 softharddecisionpd.m

```

% Soft Decision Combining for sensor nodes...
%% Initializing parameters..
close all;
clear all;
N = [100,200,300,400];% Different sum factor
k=4;% Number of Sensor Nodes
variance = [24.025e-9,23.695e-9,25.678e-9,0.0323e-9];
pfa = 0.05;%Probability of false alarm
for i=1:4
threshold(i) = (qfuncinv(pfa)+sqrt(N(i)))*sqrt(N(i))*2*variance(i);
end
% SNR Values from four sensor nodes
snrpractical = [-21.45,-18.23,-15.45,-13.3,-12.67,-9.35,-2.23,-4.32,2.98,6.95,13
.57,21.78;...
-22.23,-20.22,-17.34,-15.32,-13.45,-11.27,-7.75,-5.67,2.53,4.78
,12.67,20.32;...

```

```

-25.34,-23.34,-21.67,-20.33,-16.76,-13.38,-8.56,-6.53,0.38,1.34
,7.89,16.54;...
-27.32,-24.97,-22.34,-22.23,-17.34,-14.32,-11.35,-7.85,-2.35,-0
.98,2.38,5.98];

for i=1:4
    snrlinearprac(i,:) = 10.^ (snrpractical(i,:)/10);
end
for i=1:4
    pdprac(i,:) = qfunc((threshold(i)-2*N(i)*variance(i).* (1+snrlinearprac(i,:)))/
    ...
    (sqrt(N(i)*(1+2*snrlinearprac(i,:)))*(2*variance(i))));
end
for i=1:12
    snravg(i) = mean(snrpractical(:,i));
end
%% MNE based CS..
pdpracmne = 1-(1-pdprac(1,:)).*(1-pdprac(2,:)).*(1-pdprac(3,:)).*(1-pdprac(4,:))
;
pdpracand = mean(pdprac).^4;
pdpracm = mean(pdprac);
pdpracor = 1-(1-pdpracm).^4;
tmp1 = (1-pdpracm).^ (k-2);
tmp2 = (1-pdpracm);
pdpracmjr = (6*pdpracm.^ (k-2)).*tmp1+(4*pdpracm.^ (k-1)).*tmp2+pdpracm.^ k;
figure(1)
hold on;
grid on;
plot(snravg,pdpracmne,'-<', 'LineWidth',2, 'MarkerFaceColor','auto');
axis([-20 10 0 1])
%% EGC based CS..
snrlinearmean = 10.^ (snravg/10);
snrlinear = 10.^ (snrpractical/10);
pfa = 0.01;
M= mean(N);
threshold = mean(threshold);
for i=1:length(snravg)
    num(i) = threshold-snrlinarmean(i);

```

```

den(i) = (1/16)*((1+2*snrlinear(1,i))/N(1)+variance(1)+(1+2*snrlinear(2,i))/N(2)+variance(2)+(1+2*snrlinear(3,i))/N(3)+variance(3)+(1+2*snrlinear(4,i))/N(4)+variance(4));
pdegc(i) = qfunc(num(i)/sqrt(den(i)));
end

%% Plotting the data..
plot(snravg,pdegc,'-d','LineWidth',2,'MarkerFaceColor','auto');
plot(snravg,pdpracand,'-s','LineWidth',2,'MarkerFaceColor','auto');
plot(snravg,pdpracor,'-s','LineWidth',2,'MarkerFaceColor','auto');
plot(snravg,pdpracmjr,'->','LineWidth',2,'MarkerFaceColor','auto');
title('P_{avg} vs SNR_{avg} for Soft and Hard Decision Combining');
xlabel('SNR_{avg} in (dB)');
ylabel('Average Probability of Detection');
set(gca,'fontsize',30,'box','on','LineWidth',2,'GridLineStyle','--','GridAlpha',0.7);
legend('MNE Combining','EGC Combining','AND Rule','OR Rule','Majority Rule');

```

### A.3 spectrumsenseusrp.py

```

#!/usr/bin/env python
#
# Copyright 2005,2007,2011 Free Software Foundation, Inc.
#
# This file is part of GNU Radio
#
# GNU Radio is free software; you can redistribute it and/or modify
# it under the terms of the GNU General Public License as published by
# the Free Software Foundation; either version 3, or (at your option)
# any later version.
#
# GNU Radio is distributed in the hope that it will be useful,
# but WITHOUT ANY WARRANTY; without even the implied warranty of
# MERCHANTABILITY or FITNESS FOR A PARTICULAR PURPOSE. See the
# GNU General Public License for more details.

```

```
#  
# You should have received a copy of the GNU General Public License  
# along with GNU Radio; see the file COPYING. If not, write to  
# the Free Software Foundation, Inc., 51 Franklin Street,  
# Boston, MA 02110-1301, USA.  
  
#  
  
from gnuradio import gr, eng_notation  
from gnuradio import blocks  
from gnuradio import audio  
from gnuradio import filter  
from gnuradio import fft  
from gnuradio import uhd  
from gnuradio.eng_option import eng_option  
from optparse import OptionParser  
import sys  
import math  
import struct  
import threading  
from datetime import datetime  
import time  
from gnuradio.wxgui import stdgui2, fftsink2, form  
import wx  
  
sys.stderr.write("Warning: this may have issues on some machines+Python version  
combinations to seg fault due to the callback in bin_statistics.\n\n")  
  
class ThreadClass(threading.Thread):  
    def run(self):  
        return  
  
class tune(gr.feval_dd):  
    """  
    This class allows C++ code to callback into python.  
    """  
    def __init__(self, tb):  
        gr.feval_dd.__init__(self)
```

```

        self.tb = tb

    def eval(self, ignore):
        """
        This method is called from blocks.bin_statistics_f when it wants
        to change the center frequency. This method tunes the front
        end to the new center frequency, and returns the new frequency
        as its result.
        """

    try:
        new_freq = self.tb.set_next_freq()
        while(self.tb.msgq.full_p()):
            time.sleep(0.1)
        return new_freq

    except Exception, e:
        print "tune: Exception: ", e


class parse_msg(object):
    def __init__(self, msg):
        self.center_freq = msg.arg1()
        self.vlen = int(msg.arg2())
        assert(msg.length() == self.vlen * gr.sizeof_float)
        t = msg.to_string()
        self.raw_data = t
        self.data = struct.unpack('%df' % (self.vlen,), t)

class my_top_block(gr.top_block):
    def __init__(self):
        gr.top_block.__init__(self)

        usage = "usage: %prog [options] min_freq max_freq"
        parser = OptionParser(option_class=eng_option, usage=usage)

```

```

parser.add_option("-a", "--args", type="string", default="",
                  help="UHD device device address args [default=%default
                        ]")
parser.add_option("", "--spec", type="string", default=None,
                  help="Subdevice of UHD device where appropriate")
parser.add_option("-A", "--antenna", type="string", default=None,
                  help="select Rx Antenna where appropriate")
parser.add_option("-s", "--samp-rate", type="eng_float", default=1e6,
                  help="set sample rate [default=%default]")
parser.add_option("-g", "--gain", type="eng_float", default=None,
                  help="set gain in dB (default is midpoint)")
parser.add_option("", "--tune-delay", type="eng_float",
                  default=0.25, metavar="SECS",
                  help="time to delay (in seconds) after changing
                        frequency [default=%default]")
parser.add_option("", "--dwell-delay", type="eng_float",
                  default=0.25, metavar="SECS",
                  help="time to dwell (in seconds) at a given frequency
                        [default=%default]")
parser.add_option("-b", "--channel-bandwidth", type="eng_float",
                  default=6.25e3, metavar="Hz",
                  help="channel bandwidth of fft bins in Hz [default=%
                        default]")
parser.add_option("-l", "--lo-offset", type="eng_float",
                  default=0, metavar="Hz",
                  help="lo_offset in Hz [default=%default]")
parser.add_option("-q", "--squelch-threshold", type="eng_float",
                  default=None, metavar="dB",
                  help="squelch threshold in dB [default=%default]")
parser.add_option("-F", "--fft-size", type="int", default=None,
                  help="specify number of FFT bins [default=samp_rate/
                        channel_bw]")
parser.add_option("", "--real-time", action="store_true", default=False,
                  help="Attempt to enable real-time scheduling")

(options, args) = parser.parse_args()
if len(args) != 2:

```

```

parser.print_help()
sys.exit(1)

self.channel_bandwidth = options.channel_bandwidth

self.min_freq = eng_notation.str_to_num(args[0])
self.max_freq = eng_notation.str_to_num(args[1])

if self.min_freq > self.max_freq:
    # swap them
    self.min_freq, self.max_freq = self.max_freq, self.min_freq

if not options.realtime:
    realtime = False
else:
    # Attempt to enable realtime scheduling
    r = gr.enable_realtime_scheduling()
    if r == gr.RT_OK:
        realtime = True
    else:
        realtime = False
    print "Note: failed to enable realtime scheduling"

# build graph
self.u = uhd.usrp_source(device_addr=options.args,
                         stream_args=uhd.stream_args('fc32'))

# Set the subdevice spec
if(options.spec):
    self.u.set_subdev_spec(options.spec, 0)

# Set the antenna
if(options.antenna):
    self.u.set_antenna(options.antenna, 0)

self.u.set_samp_rate(options.samp_rate)
self.usrp_rate = usrp_rate = self.u.get_samp_rate()

```

```

    self.lo_offset = options.lo_offset

    if options.fft_size is None:
        self.fft_size = int(self.usrp_rate/self.channel_bandwidth)
    else:
        self.fft_size = options.fft_size

    self.squelch_threshold = options.squelch_threshold

    s2v = blocks.stream_to_vector(gr.sizeof_gr_complex, self.fft_size)

    mywindow = filter.window.blackmanharris(self.fft_size)
    ffter = fft.fft_vcc(self.fft_size, True, mywindow, True)
    power = 0
    for tap in mywindow:
        power += tap*tap
    c2mag = blocks.complex_to_mag_squared(self.fft_size)
    self.freq_step = self.nearest_freq((0.75 * self.usrp_rate),
                                       self.channel_bandwidth)
    self.min_center_freq = self.min_freq + (self.freq_step/2)
    nsteps = math.ceil((self.max_freq - self.min_freq) / self.freq_step)
    self.max_center_freq = self.min_center_freq + (nsteps * self.freq_step)
    self.next_freq = self.min_center_freq
    tune_delay = max(0, int(round(options.tune_delay * usrp_rate /
                                   self.fft_size))) # in fft_frames
    dwell_delay = max(1, int(round(options.dwell_delay * usrp_rate /
                                   self.fft_size))) # in fft_frames
    self.msgq = gr.msg_queue(1)
    self._tune_callback = tune(self) # hang on to this to keep it
                                    from being GC'd
    stats = blocks.bin_statistics_f(self.fft_size, self.msgq,
                                    self._tune_callback, tune_delay,
                                    dwell_delay)
    self.connect(self.u, s2v, ffter, c2mag, stats)

    if options.gain is None:

```

```

g = self.u.get_gain_range()
options.gain = float(g.start()+g.stop()) / 2.0

self.set_gain(options.gain)
print "gain =", options.gain

def set_next_freq(self):
    target_freq = self.next_freq
    self.next_freq = self.next_freq + self.freq_step
    if self.next_freq >= self.max_center_freq:
        self.next_freq = self.min_center_freq

    if not self.set_freq(target_freq):
        print "Failed to set frequency to", target_freq
        sys.exit(1)

    return target_freq


def set_freq(self, target_freq):
    """
    Set the center frequency we're interested in.

    Args:
        target_freq: frequency in Hz
        @rypte: bool
    """

    r = self.u.set_center_freq(uhd.tune_request(target_freq, rf_freq=(
        target_freq + self.lo_offset), rf_freq_policy=
        uhd.tune_request.POLICY_MANUAL))
    if r:
        return True

    return False

```

```

def set_gain(self, gain):
    self.u.set_gain(gain)

def nearest_freq(self, freq, channel_bandwidth):
    freq = round(freq / channel_bandwidth, 0) * channel_bandwidth
    return freq

def main_loop(tb):

    def bin_freq(i_bin, center_freq):
        freq = center_freq - (tb.usrp_rate / 2) + (tb.channel_bandwidth * i_bin)
        return freq

    bin_start = int(tb.fft_size * ((1 - 0.25) / 2))
    bin_stop = int(tb.fft_size - bin_start)
    fid = open("./usrp.dat", "wb")
    while 1:
        m = parse_msg(tb.msgq.delete_head())
        for i_bin in range(bin_start, bin_stop):
            center_freq = m.center_freq
            freq = bin_freq(i_bin, center_freq)
            power_db = 10 * math.log10(m.data[i_bin] / tb.usrp_rate)
            signal = m.data[i_bin] / (tb.usrp_rate)

            if (power_db > tb.squelch_threshold) and (freq >= tb.min_freq) and (
                freq <= tb.max_freq):
                print freq, signal, power_db
                fid.write(struct.pack('<f', signal))
    fid.close()#closing the file

if __name__ == '__main__':
    t = ThreadClass()
    t.start()

    tb = my_top_block()
    try:
        tb.start()

```

```

    main_loop(tb)

except KeyboardInterrupt:
    pass

```

## A.4 gnuradiortlsdrsense.py

```

#!/usr/bin/env python2
# -*- coding: utf-8 -*-

#####
# GNU Radio Python Flow Graph
# Title: DTV Spectrum Sensing
# Author: Gill
# Description: Frequency Sweep for UHF White Spaces
# Generated: Fri Mar 10 14:30:20 2017
#####

if __name__ == '__main__':
    import ctypes
    import sys
    if sys.platform.startswith('linux'):
        try:
            x11 = ctypes.cdll.LoadLibrary('libX11.so')
            x11.XInitThreads()
        except:
            print "Warning: failed to XInitThreads()"

from PyQt4 import Qt
from gnuradio import blocks
from gnuradio import eng_notation
from gnuradio import fft
from gnuradio import gr
from gnuradio import qtgui
from gnuradio.eng_option import eng_option
from gnuradio.fft import window

```

```

from gnuradio.filter import firdes
from optparse import OptionParser
import numpy as np
import osmosdr
import sip
import sys
import time

class spectrum_sensing(gr.top_block, Qt.QWidget):

    def __init__(self):
        gr.top_block.__init__(self, "DTv Spectrum Sensing")
        Qt.QWidget.__init__(self)
        self.setWindowTitle("DTv Spectrum Sensing")
        try:
            self.setWindowIcon(Qt.QIcon.fromTheme('gnuradio-grc'))
        except:
            pass
        self.top_scroll_layout = Qt.QVBoxLayout()
        self.setLayout(self.top_scroll_layout)
        self.top_scroll = Qt.QScrollArea()
        self.top_scroll.setStyle(Qt.QFrame.NoFrame)
        self.top_scroll_layout.addWidget(self.top_scroll)
        self.top_scroll.setWidgetResizable(True)
        self.top_widget = Qt.QWidget()
        self.top_scroll.setWidget(self.top_widget)
        self.top_layout = Qt.QVBoxLayout(self.top_widget)
        self.top_grid_layout = Qt.QGridLayout()
        self.top_layout.addLayout(self.top_grid_layout)

        self.settings = Qt.QSettings("GNU Radio", "spectrum_sensing")
        self.restoreGeometry(self.settings.value("geometry").toByteArray())

#####
# Variables
#####

```

```

    self.samp_rate = samp_rate = int(2e6)
    self.freq = freq = 450e6
    self.N = N = 1000

#####
# Blocks
#####
self.rtlsdr_source_0 = osmosdr.source( args="numchan=" + str(1) + " " +
    ' ')
self.rtlsdr_source_0.set_time_source('external', 0)
self.rtlsdr_source_0.set_sample_rate(samp_rate)
self.rtlsdr_source_0.set_center_freq(freq, 0)
self.rtlsdr_source_0.set_freq_corr(0, 0)
self.rtlsdr_source_0.set_dc_offset_mode(2, 0)
self.rtlsdr_source_0.set_iq_balance_mode(0, 0)
self.rtlsdr_source_0.set_gain_mode(True, 0)
self.rtlsdr_source_0.set_gain(15, 0)
self.rtlsdr_source_0.set_if_gain(15, 0)
self.rtlsdr_source_0.set_bb_gain(15, 0)
self.rtlsdr_source_0.set_antenna('', 0)
self.rtlsdr_source_0.set_bandwidth(0, 0)

self.qtgui_freq_sink_x_0 = qtgui.freq_sink_c(
    1024, #size
    firdes.WIN_BLACKMAN_hARRIS, #wintype
    0, #fc
    samp_rate, #bw
    "Recieved Signal", #name
    1 #number of inputs
)
self.qtgui_freq_sink_x_0.set_update_time(0.10)
self.qtgui_freq_sink_x_0.set_y_axis(-120, 0)
self.qtgui_freq_sink_x_0.set_y_label('Relative Gain', 'dB')
self.qtgui_freq_sink_x_0.set_trigger_mode(qtgui.TRIG_MODE_FREE, 0.0, 0,
    "")
self.qtgui_freq_sink_x_0.enable_autoscale(True)
self.qtgui_freq_sink_x_0.enable_grid(True)

```

```

    self.qtgui_freq_sink_x_0.set_fft_average(1.0)
    self.qtgui_freq_sink_x_0.enable_axis_labels(True)
    self.qtgui_freq_sink_x_0.enable_control_panel(False)

    if not True:
        self.qtgui_freq_sink_x_0.disable_legend()

    if "complex" == "float" or "complex" == "msg-float":
        self.qtgui_freq_sink_x_0.set_plot_pos_half(not True)

    labels = ['', '', '', '', '',
              '', '', '', '', '']
    widths = [2, 1, 1, 1, 1,
              1, 1, 1, 1, 1]
    colors = ["blue", "red", "green", "black", "cyan",
              "magenta", "yellow", "dark red", "dark green", "dark blue"]
    alphas = [1.0, 1.0, 1.0, 1.0, 1.0,
              1.0, 1.0, 1.0, 1.0, 1.0]
    for i in xrange(1):
        if len(labels[i]) == 0:
            self.qtgui_freq_sink_x_0.set_line_label(i, "Data {0}".format(i))
        else:
            self.qtgui_freq_sink_x_0.set_line_label(i, labels[i])
        self.qtgui_freq_sink_x_0.set_line_width(i, widths[i])
        self.qtgui_freq_sink_x_0.set_line_color(i, colors[i])
        self.qtgui_freq_sink_x_0.set_line_alpha(i, alphas[i])

    self._qtgui_freq_sink_x_0_win = sip.wrapinstance(
        self.qtgui_freq_sink_x_0.pyqwidget(), Qt.QWidget)
    self.top_layout.addWidget(self._qtgui_freq_sink_x_0_win)
    self.fft_vxx_0 = fft.fft_vcc(1024, True, (window.blackmanharris(1024)),
                                True, 1)
    self.blocks_vector_to_stream_0 = blocks.vector_to_stream(gr.sizeof_float
                                                          *1, 1024)
    self.blocks_stream_to_vector_0 = blocks.stream_to_vector(
        gr.sizeof_gr_complex*1, 1024)
    self.blocks_moving_average_xx_0 = blocks.moving_average_ff(N, 1, 4000)

```

```

self.blocks_file_sink_2_0 = blocks.file_sink(gr.sizeof_float*1, '/home/
gill/Desktop/ms-thesis/gr-spectrumsensing/grc/rtl-sdr_sensing/
Results/snr_check.dat', False)
self.blocks_file_sink_2_0.set_unbuffered(False)
self.blocks_complex_to_mag_squared_0 = blocks.complex_to_mag_squared
(1024)

#####
# Connections
#####
self.connect((self.blocks_complex_to_mag_squared_0, 0), (
    self.blocks_vector_to_stream_0, 0))
self.connect((self.blocks_moving_average_xx_0, 0), (
    self.blocks_file_sink_2_0, 0))
self.connect((self.blocks_stream_to_vector_0, 0), (self.fft_vxx_0, 0))
self.connect((self.blocks_vector_to_stream_0, 0), (
    self.blocks_moving_average_xx_0, 0))
self.connect((self.fft_vxx_0, 0), (self.blocks_complex_to_mag_squared_0,
    0))
self.connect((self.rtlsdr_source_0, 0), (self.blocks_stream_to_vector_0,
    0))
self.connect((self.rtlsdr_source_0, 0), (self.qtgui_freq_sink_x_0, 0))

def closeEvent(self, event):
    self.settings = Qt.QSettings("GNU Radio", "spectrum_sensing")
    self.settings.setValue("geometry", self.saveGeometry())
    event.accept()

def get_samp_rate(self):
    return self.samp_rate

def set_samp_rate(self, samp_rate):
    self.samp_rate = samp_rate
    self.rtlsdr_source_0.set_sample_rate(self.samp_rate)
    self.qtgui_freq_sink_x_0.set_frequency_range(0, self.samp_rate)

def get_freq(self):

```

```
    return self.freq

def set_freq(self, freq):
    self.freq = freq
    self.rtlsdr_source_0.set_center_freq(self.freq, 0)

def get_N(self):
    return self.N

def set_N(self, N):
    self.N = N
    self.blocks_moving_average_xx_0.set_length_and_scale(self.N, 1)

def main(top_block_cls=spectrum_sensing, options=None):

    from distutils.version import StrictVersion
    if StrictVersion(Qt.qVersion()) >= StrictVersion("4.5.0"):
        style = gr.prefs().get_string('qtgui', 'style', 'raster')
        Qt.QApplication.setGraphicsSystem(style)
    qapp = Qt.QApplication(sys.argv)

    tb = top_block_cls()
    tb.start()
    tb.show()

    def quitting():
        tb.stop()
        tb.wait()
    qapp.connect(qapp, Qt.SIGNAL("aboutToQuit()"), quitting)
    qapp.exec_()

if __name__ == '__main__':
    main()
```

## Appendix B

# Appendix: LTE-R Analysis Code

### B.1 kfactordist.m

```
% Calculating K-factor for the tunnel environment for HST
clear all;
close all;
clc;

%% Creating a doppler profile for high speed raiway scenario..
Ds = 30;%Initial Distance between tx and rx times 2..
Dmin = 2;% Distance between raiway tracks and leaky feeder cables...
Kf = [];
fc = 3e9;%center frequency..
c = 3e8;
v = 138.9;%300;
t = linspace(0, (2*Ds)/v(1),100);
fd = (v*fc)/3e8;%maximum doppler frequency...
costheta = zeros(size(t));%angle between BS and MS
d1 = [];
for i=1:length(t)
    d1(i) = sqrt(2^2+(Ds/2-v(1)*t(i))^2);%distance between tx and rx..
    if t(i) >=0 && t(i)<= (Ds/v)
        costheta(i) = ((Ds/2)-v*t(i))./sqrt(Dmin^2+(Ds/2-v*t(i))^2);
    end
end
```

```

elseif t(i) > (Ds/v) && t(i)<=(2*Ds)/v
costheta(i) = (-1.5*Ds+v*t(i))./sqrt(Dmin^2+(-1.5*Ds+v*t(i))^2);
end
end
fs = fd*costheta;
thetadeg = acosd(costheta);
fc_wds = fc-fs;
lambda = c./fc_wds;
Cin = 5-((0.1*1.8e10)./fc_wds)*1j;
C = Cin;
gammanum = C.*sind(thetadeg)-sqrt(Cin-(cosd(thetadeg)).^2);
gammaden = C.*sind(thetadeg)+sqrt(Cin-(cosd(thetadeg)).^2);
gamma = gammanum./gammaden;
ht = 6.1;%height of feeder cable
hr = 4.2;%height of the train
var1 = sqrt(d1.^2+(ht+hr)^2);
var2 = sqrt(d1.^2+(ht-hr)^2);
phase = (((2*pi)./lambda).* (var1-var2))*180/pi;
gammad = atan2d(imag(gamma),real(gamma));
phasegamma = abs(cosd(gammad-phase));
K = abs(gamma).^2+2*abs(gamma).*phasegamma;
Kf = 10*log10(1./K);

```

## B.2 bercalculation.m

```

% Demonstration of Eb/N0 Vs SER for M-QAM modulation scheme
clc;
load Kf;
load t;
%-----Input Fields-----
%% QPSk
bitsperframe=1e3; %Number of input symbols
EbN0dB = [linspace(0,20,50) fliplr(linspace(0,20,50))]; %Define EbN0dB range for
simulation
M=4; %for QPSk modulation.

```

```

hMod = comm.RectangularQAMModulator('ModulationOrder',M);
const = step(hMod, (0:3)');

%-----
refArray = 1/sqrt(2)*const';
k=log2(M);

totPower=15; %Total power of LOS path & scattered paths

EsN0dB = EbN0dB + 10*log10(k);
biterrsim = zeros(size(EsN0dB));
%---Generating a uniformly distributed random numbers in the set [0,1,2,...,M-1]
data=ceil(M.*rand(bitsperframe,1))-1;
s=refArray(data+1); %QPSK Constellation mapping with Gray coding
%--- Reference Constellation for demodulation and Error rate computation--
refI = real(refArray);
refQ = imag(refArray);
%---Place holder for Symbol Error values for each Es/N0 for particular M value--
index=1;
u=1;
% Kf = 4.9;
K = 10.^ (Kf/10);
for x=EsN0dB
    sn=sqrt(K(u)/(K(u)+1)*totPower); %Non-Centrality Parameter
    sigma=totPower/sqrt(2*(K(u)+1));
    h=((sigma*randn(1,bitsperframe)+sn)+li*(randn(1,bitsperframe)*sigma+0));
    numerr = 0;
    numBits = 0;
    while numerr < 100 && numBits < 1e7
        %-----
        %Channel Noise for various Es/N0
        %-----
        %Adding noise with variance according to the required Es/N0
        noiseVariance = 1/(10.^ (x/10));%Standard deviation for AWGN Noise
        noiseSigma = sqrt(noiseVariance/2);
        %Creating a complex noise for adding with M-QAM modulated signal
        %Noise is complex since M-QAM is in complex representation
        noise = noiseSigma*(randn(size(s))+li*randn(size(s)));
        received = s.*h + noise;

```

```

%-----I-Q Branching-----
received = received./h;
r_i = real(received);
r_q = imag(received);
%---Decision Maker-Compute  $(r_i - s_i)^2 + (r_q - s_q)^2$  and choose the
smallest
r_i_repmat = repmat(r_i,M,1);
r_q_repmat = repmat(r_q,M,1);
distance = zeros(M,bitsperframe); %place holder for distance metric
minDistIndex=zeros(bitsperframe,1);
for j=1:bitsperframe
    %---Distance computation -  $(r_i - s_i)^2 + (r_q - s_q)^2$  -----
    distance(:,j) = (r_i_repmat(:,j)-refI').^2+(r_q_repmat(:,j)-refQ').
        ^2;
    %---capture the index in the array where the minimum distance occurs
    [dummy,minDistIndex(j)]=min(distance(:,j));
end
y = minDistIndex - 1;
%-----Symbol Error Rate Calculation
-----
dataCap = y;
numerr = sum(dataCap~=data)+numerr;
numBits = numBits+bitsperframe;
disp(numerr);
end
symErrSimulatedqpsk(1,index) = numerr/numBits;
biterrsime(1,index) = symErrSimulatedqpsk(1,index)/k;
index=index+1;
% u=u+1;
end

%% 16 QAM
bitsperframe=1e3; %Number of input symbols
EbN0dB = [linspace(0,10,50) fliplr(linspace(0,10,50))]; %Define EbN0dB range for
simulation
M=16; %for QPSK modulation.
hMod = comm.RectangularQAMModulator('ModulationOrder',M);

```

```

const = step(hMod, (0:M-1)');
%-----
refArray =1/sqrt(10)*const';
k=log2(M);
totPower=10; %Total power of LOS path & scattered paths

EsN0dB = EBN0dB + 10*log10(k);
biterrsim = zeros(size(EsN0dB));
%---Generating a uniformly distributed random numbers in the set [0,1,2,...,M-1]
data=ceil(M.*rand(bitsperframe,1))-1;
s=refArray(data+1); %QPSK Constellation mapping with Gray coding
%--- Reference Constellation for demodulation and Error rate computation--
refI = real(refArray);
refQ = imag(refArray);
%---Place holder for Symbol Error values for each Es/N0 for particular M value--
index=1;
u=1;
K = 10.^ (Kf/10);
for x=EsN0dB
    numerr = 0;
    numBits = 0;
    while numerr < 100 && numBits < 1e7
        sn=sqrt(K(u) / (K(u)+1)*totPower); %Non-Centrality Parameter
        sigma=totPower/sqrt(2*(K(u)+1));
        h=((sigma*randn(1,bitsperframe)+sn)+li*(randn(1,bitsperframe)*sigma+0));
        %-----
        %Channel Noise for various Es/N0
        %-----
        %Adding noise with variance according to the required Es/N0
        noiseVariance = 1/(10.^ (x/10));%Standard deviation for AWGN Noise
        noiseSigma = sqrt(noiseVariance/2);
        %Creating a complex noise for adding with M-QAM modulated signal
        %Noise is complex since M-QAM is in complex representation
        noise = noiseSigma*(randn(size(s))+li*randn(size(s)));
        received = s.*h + noise;
        %-----I-Q Branching-----

```

```

received = received./h;
r_i = real(received);
r_q = imag(received);
%---Decision Maker-Compute  $(r_i - s_i)^2 + (r_q - s_q)^2$  and choose the
smallest
r_i_repmat = repmat(r_i,M,1);
r_q_repmat = repmat(r_q,M,1);
distance = zeros(M,bitsperframe); %place holder for distance metric
minDistIndex=zeros(bitsperframe,1);
for j=1:bitsperframe
%---Distance computation -  $(r_i - s_i)^2 + (r_q - s_q)^2$  -----
distance(:,j) = (r_i_repmat(:,j)-refI').^2+(r_q_repmat(:,j)-refQ').
^2;
%---capture the index in the array where the minimum distance occurs
[dummy,minDistIndex(j)]=min(distance(:,j));
end
y = minDistIndex - 1;
%-----Symbol Error Rate Calculation
-----
dataCap = y;
numerr = sum(dataCap~=data)+numerr;
numBits = numBits+bitsperframe;
disp(numerr);
end
symErrSimulatedqam(l,index) = numerr/numBits;
biterrsime(l,index) = symErrSimulatedqam(l,index)/k;
index=index+1;
u=u+1;
end

%% 64 QAM Modulation...
bitsperframe=1e3; %Number of input symbols
EbN0dB = [linspace(0,10,50) fliplr(linspace(0,10,50))]; %Define EbN0dB range for
simulation
M=64; %for QPSK modulation.
hMod = comm.RectangularQAMModulator('ModulationOrder',M);
const = step(hMod, (0:M-1)');

```

```
%-----
refArray =1/sqrt(42)*const';
k=log2(M);
totPower=10; %Total power of LOS path & scattered paths
EsN0dB = EbN0dB + 10*log10(k);
biterrsime = zeros(size(EsN0dB));
%---Generating a uniformly distributed random numbers in the set [0,1,2,...,M-1]
data=ceil(M.*rand(bitsperframe,1))-1;
s=refArray(data+1); %QPSK Constellation mapping with Gray coding
%--- Reference Constellation for demodulation and Error rate computation--
refI = real(refArray);
refQ = imag(refArray);
%---Place holder for Symbol Error values for each Es/N0 for particular M value--
index=1;
u=1;
K = 10.^ (Kf/10);
for x=EsN0dB
    sn=sqrt(K(u) / (K(u)+1)*totPower); %Non-Centrality Parameter
    sigma=totPower/sqrt(2*(K(u)+1));
    h=((sigma*randn(1,bitsperframe)+sn)+1i*(randn(1,bitsperframe)*sigma+0));
    numerr = 0;
    numBits = 0;
    while numerr < 100 && numBits < 1e7
        %-----
        %Channel Noise for various Es/N0
        %-----
        %Adding noise with variance according to the required Es/N0
        noiseVariance = 1/(10.^(x/10));%Standard deviation for AWGN Noise
        noiseSigma = sqrt(noiseVariance/2);
        %Creating a complex noise for adding with M-QAM modulated signal
        %Noise is complex since M-QAM is in complex representation
        noise = noiseSigma*(randn(size(s))+1i*randn(size(s)));
        received = s.*h + noise;
        %-----I-Q Branching-----
        received = received./h;
        r_i = real(received);
        r_q = imag(received);
```

```

%---Decision Maker-Compute  $(r_i-s_i)^2+(r_q-s_q)^2$  and choose the
smallest
r_i_repmat = repmat(r_i,M,1);
r_q_repmat = repmat(r_q,M,1);
distance = zeros(M,bitsperframe); %place holder for distance metric
minDistIndex=zeros(bitsperframe,1);
for j=1:bitsperframe
    %---Distance computation -  $(r_i-s_i)^2+(r_q-s_q)^2$  -----
    distance(:,j) = (r_i_repmat(:,j)-refI').^2+(r_q_repmat(:,j)-refQ').
        ^2;
    %---capture the index in the array where the minimum distance occurs
    [dummy,minDistIndex(j)]=min(distance(:,j));
end
y = minDistIndex - 1;
%-----Symbol Error Rate Calculation
-----
dataCap = y;
numerr = sum(dataCap~=data)+numerr;
numBits = numBits+bitsperframe;
disp(numerr);
end
symErrSimulatedqam64(1,index) = numerr/numBits;
biterrsime(1,index) = symErrSimulatedqam64(1,index)/k;
index=index+1;
u=u+1;
end

%%
fig = figure;
semilogy(t*1e3,symErrSimulatedqpsk(1,:),'-d','LineWidth',2);
hold on;
grid on;
semilogy(t*1e3,symErrSimulatedqam(1,:),'-d','LineWidth',2);
semilogy(t*1e3,symErrSimulatedqam64(1,:),'-d','LineWidth',2);
xlabel('Time (ms)');
ylabel('Bit Error Rate (Pb)');
title(['BER For OFDM Under Rician Fading Environment Inside Tunnel']);

```

```
set(gca,'fontsize',30,'box','on','LineWidth',2,'GridLineStyle','--','GridAlpha'  
,0.7);  
axis([0 max(t)*1e3 10e-7 0])  
lgd = legend('QPSK','16QAM','64QAM');  
lgd.FontSize=20;
```